

**MEASUREMENTS OF MAGNETOCRYSTALLINE ANISOTROPY
AND MAGNETIZATION OF NICKEL**

BY

MD. TAHIDUL HAQUE



**A THESIS SUBMITTED TO THE DEPARTMENT OF PHYSICS
BANGLADESH UNIVERSITY OF ENGINEERING & TECHNOLOGY
IN PARTIAL FULFILMENT OF THE REQUIRMENT FOR THE DEGREE OF
MASTER OF PHILOSOPHY**

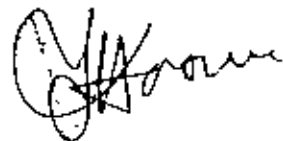


**BANGLADESH UNIVERSITY OF ENGINEERING & TECHNOLOGY
DHAKA, BANGLADESH**

November 1998

DECLARATION

This thesis work has been done by the candidate himself. The work for this thesis has not been presented elsewhere by the author for any degree or diploma. No other person's work has been used or included without due acknowledgement.



(Md. Fahidul Haque)
Candidate

Certificate

This is to certify that the research work embodying in this thesis has been carried out under my supervision. The work presented herein is original. This thesis has not been submitted elsewhere for the award of any degree or diploma in any other University.



Dr. Md. Feroz Alam Khan
Supervisor

Assistant Professor

Department of Physics

Bangladesh University of

Engineering & Technology

Dhaka 1000, Bangladesh

Bangladesh University of Engineering & Technology
Department of Physics

Certification of Thesis Work

A Thesis On

“Measurements of Magnetocrystalline Anisotropy and Magnetization of Nickel”

BY

Md. Tahidul Haque

has been accepted as satisfactory in partial fulfilment for the degree of Master of
Philosophy in Physics and certify that the student demonstrated a satisfactory
knowledge of the field covered by this thesis in an oral examination held on
3rd January, 1999

Board of Examiners

1. Dr. Md. Feroz Alam Khan
Assistant Professor
Department of Physics
BUET, Dhaka




Supervisor & Chairman

2. Prof. Dr. Mominul Haq
Head, Department of Physics
BUET, Dhaka



Member

3. Prof. Dr. M. Ali Asgar
Department of Physics
BUET Dhaka



Member

5. Prof. Dr. Ajoy Kumar Roy
Department of Physics
University of Dhaka
Dhaka



Member (External)

Acknowledgement

First of all, I would like to offer my grateful thanks to my supervisor Dr. Md. Feroz Alam Khan for introducing me to the exciting field of magnetism and guiding me actively through to the end of this work. Having embarked on this project I would never have completed it without the tireless efforts and unbounded enthusiasm of Dr. Khan.

I am grateful to Prof. Mominul Huq, Head, Department of Physics, BUET, for his inspiration and helpful suggestions.

I am thankful to Prof. M. Ali Asgar from whom I learned a lot of basic things on magnetism

I express my thanks to Prof. Gias Uddin Ahmad and Prof. Tafazzal Hossain for their kind co-operation and inspiration during this work

I would like to thank Dr. Abu Hashan Bhuiyan, Mrs. Dil Afroze Ahmed, Dr. Nazma Zaman, Mrs. Fahima Khanam, Dr. Jiban Podder, Dr. Nazrul Islam, Mr. Md. Ashrafuzzaman, and Ms. Afia Begum for their co-operation.

I am also thankful to Mr. Amanullah Chowdhury (P.S.O) and Dr. A. K. M. Abdul Hakim (P.Eng) of the Magnetic Materials Division of the Bangladesh Atomic Energy Commission (AECD), Dhaka, for allowing me to use the VSM.

I have deep sense of gratitude to three Ph. D. students of the Department of Physics, BUET, namely, Mr. A. J. Saleh Ahmed Khandaker, Mr. Shibendra Shekhar Sikder and Mr. Faruque-uz-zaman Chowdhury for their co-operation during my research in the Solid State Physics Laboratory of BUET.

My special thanks are offered to my friends Badal, Jamal, Tapan, Farid, Manju, Mosarraf, Razzak, Mokammel, Shuva and Shyamal for their help and care.

Thanks to my parents, brothers and loving sister for being so patient caring and keeping my spirits up. Without their moral support, this work would not have been finished unhindered.

I am very much thankful to the authority of BUET for giving me the opportunity of research and the financial support for my work.

Abstract

This thesis describes the experimental investigation of magnetocrystalline anisotropy and magnetization of Nickel single crystal. The first anisotropy constants have been determined at different temperatures. The anisotropy constants have been determined by torque measurements in the (100) crystallographic plane as a function of fields and temperatures. The measurements are performed using a Torque Magnetometer with automatic electronic compensating system. The temperature dependence of magnetic anisotropy of Ni is found to comply with the earlier works on this magnetic system. A rotation of the magnetic vector is predicted around the ferromagnetic Curie temperature T_c . As the sample entered in to the paramagnetic phase, some non-periodic signals are recorded, the cause of which may be attributed to the local spin fluctuations in the unbroken clusters containing ferromagnetically ordered spins near the onset of paramagnetic phase. The magnetization of the sample is measured by a Vibrating Sample Magnetometer (V.S.M). The variation of the anisotropy constants due to change of temperature is found to be faster than the variation of magnetization in Nickel.

Contents:	Page
Chapter 1 Introduction	1
Chapter 2 Review of earlier works	3
Chapter 3 Magnetism in solids	11
3.1 Paramagnetism	11
3.2 Ferromagnetism	12
3.2.1 The molecular field model of ferromagnetism	18
3.2.2 The localised electron model	19
3.3 Antiferromagnetism	23
Chapter 4 Magnetic anisotropy	25
4.1 Theories based on localized electron model	25
4.2 Pair model of magnetic anisotropy	28
4.3 Single-ion model of magnetic anisotropy	33
4.4 Physical origin of magnetocrystalline anisotropy	37
4.5 The temperature dependence of magnetocrystalline anisotropy	40
4.6 Magnetocrystalline anisotropy of Nickel	46
4.7 Different measurement techniques of magnetic anisotropy	47
4.7.1 Ferromagnetic resonance method	47
4.7.2 Magnetic torque method	48
4.7.3 Magnetization method	49
Chapter 5 Experimental	52
5.1 The torque measurement	52
5.2 Design and working principle of the Torque Magnetometer	56
5.3 Measurement of magnetic anisotropy by Torque Magnetometer	58
5.4 Sample preparation	59
5.5 The sample suspension	60
5.6 Calibration of the Torque Magnetometer	60
5.7 The High Temperature Oven	61

5.8	Evaluation of the torque curve by Fourier analysis	64
5.9	Magnetization process of Nickel	64
5.10	The working principle of the Vibrating Sample Magnetometer (VSM)	67
5.11	Description of mechanical design of the VSM	69
5.12	Calibration of the VSM	72
5.14	Measurement of magnetization of Nickel by VSM	73
5.15	Evaluation of magnetic moment data of Nickel	74
Chapter 6	Result and Discussion	75
	Conclusion	86
	Appendix	
	References	

Chapter 1

Introduction



The magnetocrystalline anisotropy is a secondary effect which characterises the magnetic softness or hardness. In practical application almost all the devices using magnetic material as a core material demand that the material be magnetically soft and isotropic so that the hysteresis loss is minimum. The area under a B-H loop indicates the magnetic softness or hardness of a magnetic material. Thus minimising the area inside a B-H loop has long been the focus of magnetic research.

One factor which may strongly affect the shape of the M, H (or B, H) curve or the hysteresis loop is the magnetic anisotropy. This term simply means that the magnetic properties depend on the direction in which they are measured. So it is one of the most important characteristics which determine the complex magnetization process of an ordered magnetic material. This general subject is of considerable practical interest, because minimising the magnetic anisotropy is very important while we design most of the devices of commercial importance using magnetic materials.

The present theoretical knowledge of the origin of magnetic anisotropy is not quite clear as there are various factors on which this property of a magnetic material depend. The atomic structure of a material is at thermodynamic equilibrium when the atoms take the positions to minimise its energy. Iron having the body centred cubic (b.c.c) structure could be easily magnetized along the $[100]$ crystallographic direction. On the otherhand Nickel having the face centred cubic structure (f.c.c) could be easily magnetized along the $[111]$ crystallographic (body diagonal) direction.

The physical properties of a ferromagnetic single crystal in general depends on the direction along which their magnetization is measured relative to the crystal axes. In a ferromagnetic single crystal there is preferred crystallographic direction along which it is easily magnetized which is known as the easy direction of magnetization. There is also a hard direction along which it is difficult to magnetize. The difference in energy

to magnetise the sample in the hard and easy directions is a measure of the magnetocrystalline anisotropy. The reason for the magnetic anisotropy may be attributed to the stacking of the atoms taking the minimum energy position during their growth. Thus as one passes through a crystalline arrangement of atoms or molecules along a given direction, one meets atoms or group of atoms having minimum energy orientations.

The magnetic anisotropy in a ferromagnetic material and also in their alloys may be induced by mechanical stress which is called the induced anisotropy. The magnetic anisotropy in a metallic glass ribbon is an example of induced magnetic anisotropy. The mechanical stress suffered by the ribbon during its growth gives rise to the induced magnetic anisotropy.

Cobalt has higher anisotropy energy than Iron and Nickel. When an external magnetic field is applied on a magnetic material the magnetization vector tries to rotate and align itself with the external field. This happens as the electron spin moments try to rotate along with the applied magnetic field. But this effort of rotation is resisted by the electron orbits as they are strongly bound to the crystal field created by the lattices. As the lattices are strongly bound in a crystal, the electron moments can not rotate them. However, if a strong external magnetic field is applied, the strong bindings between the lattices and the electron spins could be overcome. The amount of energy required to overcome this binding is the magnetocrystalline anisotropy energy whose underlying reason is the spin-orbit coupling.

Magnetocrystalline anisotropy of Nickel which is the main aspect of present research is evaluated from the torque curves, and also its temperature dependence is studied from room temperature to and above the ferromagnetic Curie temperature T_c .

Chapter 2

Review of Earlier Works

Study of magnetocrystalline anisotropy and magnetostriction has long been the subject of research by the Scientists who are working for the development of magnetic materials for scientific and industrial applications. The magnetically soft and hard materials are characterised on the basis of their hysteresis. The soft magnetic materials are identified by their small hysteresis loss. When such magnetic materials are used in sophisticated electronic devices powered by small batteries, they usually consume very small power from the source. To minimise the hysteresis losses and to preserve their useful magnetic properties have been quite a challenging task in recent days of technological revolution. Thus the study of magnetocrystalline anisotropy and magnetostriction is one of the very important fields in magnetic research

The classical theory of ferromagnetic anisotropy in cubic crystals was formulated by Akulov [1]. He showed that if the anisotropy energy is expanded in powers of the direction cosines α_1 , α_2 , and α_3 between the bulk magnetization vector and the three cubic axes, the lowest non-vanishing term must be of the form

$$K_1 = K_1(\alpha_1^2 \alpha_2^2 + \alpha_2^2 \alpha_3^2 + \alpha_3^2 \alpha_1^2) \quad \dots\dots\dots(2.1)$$

A rough estimate of the temperature dependence of the first anisotropy constant K_1 was also given by Akulov. He considered the crystal to be composed of a number of small regions, and within each region he assumed that the magnetization vector makes a random small angle θ with respect to the average over-all direction of bulk magnetization. As the temperature increases, the angle θ between regional and average magnetization becomes larger and larger, and the total anisotropy energy drops precipitously. At a stage the total anisotropy energy will disappear; however, the

sample magnetization $M(T)$, which is given by the average value of M_i , will be quite large. Akulov derived the expression

$$\frac{K_1(T)}{K_1(0)} = 1 - 10 \frac{[M(0) - M(T)]}{M(0)} \dots\dots\dots(2.2)$$

In 1954 C. Zener [2] in Westinghouse Research Laboratory, attempted to understand the temperature dependence of the crystal anisotropy. In his attempt he proceeded in a classical manner with two assumptions: (i) the effect of temperature upon magnetic anisotropy arises solely from the introduction of local deviation in the direction of magnetization; and (ii) The local deviation in an elementary region is the resultant of a very large number of independent deviations. He saw that the anisotropy in nickel decreases much more rapidly than predicted and found that K_1 decreases at least twice as rapidly with T/T_c in the case of nickel as in the case of iron. Since J_c decreases in approximately the same manner for those two metals, he concluded that the same agreement would not be obtained for nickel as was obtained for iron. Zener has shown by random-walk calculation of the average angle θ that a more precise formulation of eq (2.2) is a "10th power law"

$$\frac{K_1(T)}{K_1(0)} = \left[\frac{M(T)}{M(0)} \right]^{10} \dots\dots\dots(2.3)$$

a result which fits excellently to the experimental curve for iron, but fails completely in the case of nickel where one finds approximately

$$\frac{K_1(T)}{K_1(0)} = \left[\frac{M(T)}{M(0)} \right]^{21} \dots\dots\dots(2.4)$$

Robert Brenner [3] found the reason why the proposed model should hold for iron only. He showed that the tenth power of $M(T)/M(0)$ holds for all temperatures up to the Curie point.

Zener has given a general expression for higher-order anisotropy. In particular, the temperature dependence of K_2 is as close to the 21st power of $M(T)$. Zener has also shown that if $K_2(0)$ is of comparable magnitude to $K_1(0)$, K_1 increases as the temperature falls off.

The Akulov-Zener macroscopic classical theory is quite general, and seems to be a correct first approximation regardless of the type of microscopic quantum-mechanical source of the anisotropy. The standard quantum-mechanical theory has been given by Van Vleck [4]. He has expanded the indirect anisotropic coupling between neighbour spins into a dipole-dipole term

$$H_D = \sum_{ij} D_{ij} [S_i \cdot S_j - 3r_{ij}^{-2} (S_i \cdot r_{ij})(S_j \cdot r_{ij})], \quad \dots\dots\dots(2.5)$$

plus a quadrupole-quadrupole term

$$H_Q = \sum_{ij} Q_{ij} r_{ij}^{-4} (S_i \cdot r_{ij})^2 (S_j \cdot r_{ij})^2 \quad \dots\dots\dots(2.6)$$

Here r_{ij} connects nearest neighbours, i.e., spin i and spin j and D_{ij} and Q_{ij} are the coupling constants, which is considered temperature independent and acting only between nearest neighbours.

In the Van Vleck theory the temperature dependence of the macroscopic anisotropy is caused by statistical deviations of S_i and S_j from maximum alignment. Because he evaluated these deviations in a molecular field, that is, assuming complete lack of correlation in the alignment of neighbouring spins; Van Vleck obtained too slow a temperature dependence of K_1 . It has been shown by Keffer [5] that if correlation is properly taken into account, Van Vleck's H_Q leads to the 10th power law. This may be demonstrated in a general way, and also by means of a spin-wave analysis. Pal [6] has

independently made a spin-wave calculation leading to an equivalent result. In an excellent review article Van Vleck [7] has exhibited a very powerful and completely general extension of correlation concept. Thus the anisotropy arising from H_Q behaves according to the Akulov-Zener theory, and the quadrupolar-coupling problem is well-understood.

Van Vleck's second order perturbation theory of dipolar type anisotropy in cubic ferromagnets was re-evaluated by F. Keffer and T. Ogueli [8] and Frederic Keffer [9]. Essentially the same correlation was obtained very easily from a simple modification of the Van Vleck formalism to take careful account of the average energy involved in simultaneous reversal of neighbouring spins. It was shown that the spin-wave theory, in agreement with classical theory, predicts identical values of dipolar-type anisotropy whether measured statically in a torque experiment or dynamically in a microwave resonance experiment.

R. R. Birss and P. M. Wallis [10] had worked on the temperature dependence of magnetocrystalline anisotropy. They have shown that the tenth power law $\frac{K_1(T)}{K_1(0)} = \left[\frac{M_s(T)}{M_s(0)} \right]^{10}$ is in much better agreement with experiment at low temperature.

The theory of temperature dependence of magnetocrystalline anisotropy in ferromagnetic insulators was reviewed and summarized by H. B. Callen and E. Callen [11]. They found that the derivation of the 10th power law is restricted to materials with localized spins and $3d$ metals are almost surely exempted. For various insulating magnetic materials and even for rare earth metals the experimental data, which they reviewed was in excellent agreement with the $l(l+1)/2$ power law. They also saw that the theory of the temperature dependence of the anisotropy could be extended to arbitrary temperatures and it stood in excellent agreement with the data for insulating materials. They also discussed the magnetic field dependence of magnetic anisotropy.

In 1968 J. J. M. Franse and G. De Vries [12] attempted to measure the magnetocrystalline anisotropy energy of nickel at different temperatures between 1.5 K and 296 K. They based their description on the usual expansion of this energy:

$$E_4 = K_0 + K_1s + K_2p + K_3s^2 + K_4sp + K_5s^3 + K_6p^2 + \dots \quad \dots\dots(2.7)$$

where $s = \alpha_1^2\alpha_2^2 + \alpha_2^2\alpha_1^2 + \alpha_3^2\alpha_1^2$ and $p = \alpha_1^2\alpha_2^2\alpha_3^2$; α_1 , α_2 and α_3 being the direction cosines of the magnetization with respect to the crystal axis and K_1 , K_2 etc the anisotropy constants. These constants were derived from torque measurements by a least adjustment. Neglecting higher constants they got, however, a good estimation of K_2 and with the aid of this constant they attempted to determine K_1 , K_2 and K_3 from the combined torque curves in the (100), (110) and (111) planes.

R. R. Birss, G. J. Keeler and P. D. Leo [13] measured the anisotropic magnetization (M_i) of nickel by a rotating sample magnetometer over a range of temperature from 4K to 250K. A new technique of analysis was used which reveals that the effect is field dependent at low fields. In all cases the field dependence of K_i were found to be essentially the same at all fields, but M_i showed a marked field dependence.

R. M. Bozorth [14] showed that by taking account of an additional term in the expression for the energy of magnetization the [110] direction might under certain conditions be the direction for easy magnetization in a crystal, instead of [100] or [111]. Magnetization curves for single crystals were calculated using the additional term.

L. P. Tarasov [15] worked a lot over the dependence of ferromagnetic anisotropy on the field strength. By using a torquemeter of very high sensitivity, he had been able to show that a saturation value of the torque could not be obtained experimentally, but could be calculated by extrapolating to $\frac{1}{H} = 0$. The result is expressed by the equation

$$T_H = T_\infty \left[1 - \frac{H_0}{H} \right] \quad \dots\dots(2.8)$$

where T_H and T_∞ are the magnitudes of the torque peaks for an applied field H_a and for an infinite one respectively, and H_0 is a constant. The usefulness of the $\frac{1}{H}$ law for disks lies in the fact that it makes possible the calculation of a unique value of the



anisotropy constant, the one corresponding to $\frac{1}{H} = 0$, which neither depends upon the field used nor upon the dimensions of the specimen.

When a disk cut from a cubic crystal of a ferromagnetic material is placed in a magnetic field parallel to its plane, the torque exerted on the disk by the field generally increases continually with the strength of the field, approaching a finite limit (saturation) in very high fields. An anomaly for one orientation of a crystal of iron-silicon was observed by Tarasov. R. M. Bozorth and H. J. Williams [16] confirmed his findings and observed a similar effect for a series of orientations of disks cut parallel to the (110) and (100) planes. As the field strength is increased, the torque passes through a well-defined maximum before beginning the final approach to saturation.

C. D. Graham [17] reported precise measurements below room temperature which indicate in this range not a tenth power, but fourth or fifth power dependence on magnetization. W. J. Carr [18] interpreted this seemingly anomalous result for the temperature dependence of magnetic anisotropy in ferromagnetic material on the basis of Zener's theory, with the effect of thermal expansion.

The conventional theory of the variation with temperature of the anisotropy of cubic crystals is extended by C. Kittel and J. H. Van Vleck [19] to include the magnetoelastic constants. Their results are expressed in the form of a functional relation connecting the magnetoelastic energy with M rather than T , but as the saturation magnetization M is itself a function of T , the form of dependence on T is in principle determined. Hecker and Döring [20] showed the magnetoelastic energy in a cubic crystal by symmetry considerations.

W. J. Carr, [21] worked a lot to develop the theory of ferromagnetic anisotropy. It is generally agreed that the principal source of ferromagnetic anisotropy in most materials, particularly metals, comes from electronic spin-orbit coupling, a suggestion seems first to have been advanced by Powell [22], and later in a more concrete form by Bloch and Gentile [23]. Two note-worthy schemes have been used in attempting to calculate the effect of spin-orbit interaction in a ferromagnetic solid; one by Van Vleck

[24] using an atomic approach, the other by Brooks [25] using an energy-band approximation. Later using an improved energy-band model, Fletcher [26] gave a result for nickel two orders of magnitude too large. But one of the principal mechanisms for anisotropy was found by Carr to be different from those considered by Van Vleck, and arises from the interaction between the orbital moment about a lattice site and the crystalline potential of the lattice.

W. J. Carr [27] also verified the temperature dependence of crystalline anisotropy constants of iron, cobalt, and nickel. He showed that Zener's result for iron (i.e. the first anisotropy constant varies as the tenth power of the magnetization) also might be derived from molecular field theory. In cobalt a satisfactory agreement with experiment was obtained by using Zener's results together with the postulate that the intrinsic anisotropy varies with thermal expansion. For nickel the temperature dependence of K_1 seemed to require, in addition to the tenth power of magnetization, a multiplicative factor that is linear in the temperature.

F. C. Nix and D. MacNair [28] investigated the thermal expansion of pure metals. Their values for these characteristic temperatures are: $410K$ for *Ni* and $420K$ for *Fe*. The ferromagnetic Curie temperature is found to be $625K$. In plotting true coefficient of thermal expansion versus temperature Simon and Bergmann [29] found a horizontal plateau at about $175K$ to $235K$ for *Ni* and *Fe*.

The ferromagnetic anisotropy constant K_1 was accurately measured by the magnetic torque method for a group of iron alloys containing up to 13.7 atomic percent silicon by L. P. Tarasov [30]. The value for iron was considerably higher than the one due to Akulov [31]. When K_1 is plotted against the atomic percentage of silicon, the change in slope occurs at very nearly the same concentration as the similar change in slope found by Jette and Greiner [32] for the lattice parameter a_0 . An attempt was made to explain the occurrence of these breaks in terms of change from a hypothetical superlattice with a silicon concentration of $3/32$ to a partially formed Fe_3Si superlattice.

Since K_1 values are often required for the theoretical treatment of the problem, a new, and direct, determination of K_2 for iron and nickel was made by Hiroshi Sato and B. S. Chandrasekhar [33] by means of magnetic torque measurements in the (111) plane. This method minimizes the contribution from K_1 to the torque. Then the pure K_2 contribution was singled out from the measured torque curve with the aid of symmetry considerations. The values obtained for iron and nickel are at room temperature $7.14 \times 10^3 \text{ J/m}^3$ and $2.34 \times 10^4 \text{ J/m}^3$ respectively. The results show, in the case of iron, that the value of K_2 which had been given previously with the same order of magnitude as K_1 , is actually an order of magnitude smaller. In the case of nickel, the value is comparable to K_1 and its temperature dependence is even larger than that of K_1 .

The conventional theory of the variation with temperature of the anisotropy of cubic crystals has been used to calculate the magneto-elastic constants [34].

L. Néel, R. Pauthenet, G. Rinet, and V. S. Giron [35] described the mechanism of magnetization of a ferromagnetic single crystal. They classified the elementary domains in several groups, called "phases" each having a certain direction of the spontaneous magnetization. The variation of the total magnetization took place in various "modes," corresponding to the number of coexisting phases in a given field. The calculation of the magnetization curve in these various modes explains the experimental results for single crystals.

Chapter 3

Magnetism in Solids

3.1 Paramagnetism

When the magnetic atoms in a substance are non-interacting and are not affected by any spontaneous internal field, it is said to be a paramagnetic state. It is related to the tendency of a permanent magnet to align itself in the direction of magnetic field such that its dipole moment is parallel to the field. In atomic systems the permanent magnetic moment is associated with the electronic spin as in all atoms, molecules and lattice defects possessing an odd number of electrons, the total spin cannot be zero. Thus a paramagnetic substance has a non-vanishing angular momentum. It may also be the permanent moment of unfilled atomic shells that arises from the combination of spin and orbital moment.

Some atoms and ions have permanent magnetic moments. In the absence of a magnetic field, these moments usually point in random directions and hence produce no macroscopic magnetization. But in the presence of magnetic field, the moments tend to line up preferentially in the field direction and produce a net magnetization. The perfect alignment is classically possible at infinite magnetic field. Since the moments line up in the direction of the field and enhance the external field, the susceptibility is greater than zero.

Paramagnetism is thus found in those materials where the individual atoms, ions or molecules have a permanent magnetic dipole moment but no molecular field. Mn^{2+} , Gd^{3+} , U^{4+} are the examples of paramagnetic materials. According to Hund's rule, in a partly filled transition metal, the various orbital states are filled first by electrons of one spin, then by the other, so that pairing of electron spins is the least possible and the spin magnetic moment is maximised. It is this type of exchange interaction that is

responsible for spin alignment in paramagnetic materials. Paramagnetism may also arise from atoms, ions or molecules with a net magnetic dipole moment. It is observed experimentally that for many materials in weak magnetic fields, the susceptibility is inversely proportional to temperature. This dependence of susceptibility on temperature is known as Curie's law. According to this law the susceptibility χ is defined as

$$\chi_{\text{param}} = \mu_0 \frac{M}{B} = \frac{C}{T} \quad \dots\dots\dots(3.1)$$

where C is the Curie constant.

3.2 Ferromagnetism

A metal is composed of atoms. The magnetic moment of an atom is associated with the spin motion of its electrons and their orbital motion around the nucleus. The magnetic orbital quantum number m_l and the magnetic spin quantum number m_s determine the quantum state of an atom. For a filled shell of an atom the contribution from both the orbital and spin motion is zero, i.e., $\sum m_l = 0$ and $\sum m_s = 0$. This is the situation for complete diamagnetism where all the atomic shells are filled. On the other hand in the case of 3d transition elements the shells are not completely filled and there are resultant $\sum m_l$ and $\sum m_s$, which are non-zero.

This means that they have a resultant magnetic moment. These materials when subjected to external magnetic field exhibit very large magnetization. This magnetization is not reversible and persists even after the magnetic field is withdrawn.

When cooled below a certain critical temperature, the magnetic moments of the atoms are ordered to a certain degree even in the absence of an external magnetic field. Ferromagnetic materials are characterised by the presence of spontaneously magnetized regions called domains and the existence of internal molecular field B_i as proposed by Weiss (1907). The origin of the molecular field was explained by Heisenberg (1924) and the existence of domains was explained by Landau and Lifshitz. At 0K or at infinite magnetic field the alignment of the spins is complete and the magnetization attains its maximum value. Materials like transition metals *Fe*, *Co*, *Ni* and some rare-earth metals like *Gd* and oxides *CrO₂*, *ErO* are examples of ferromagnetic materials.

The field seen by an atomic dipole is the sum of the applied field B_0 and the internal field B_i i.e.,

$$B = B_0 + B_i \quad \dots \dots \dots (3.2)$$

where $B_i = \lambda M$ and λ is known as the Weiss constant.

If B is such that $\frac{g\mu_B B}{k_B T}$ is small, where g is the Lande 'g'-factor, μ_B is the Bohr magneton and k_B is the Boltzmann constant. Then we can write

$$\begin{aligned} \chi_{ferro}^m &= \mu_0 \frac{M}{B_0} = \frac{Ng^2 \mu_B^2 J(J+1)}{8k_B T} \left(1 + \frac{\lambda M}{B_0}\right) \\ &= \frac{C}{T} \left(1 + \frac{\lambda \chi_{ferro}^m}{\mu_0}\right) \end{aligned}$$

where

$$C = \frac{Ng^2 \mu_B^2 J(J+1)}{8k_B}$$

or

$$\chi_{ferro}^m = \frac{C}{T - T_c} \quad \dots \dots \dots (3.3)$$

where

$$T_c = \frac{C\lambda}{\mu_0}$$

T_c is the Curie temperature at which the susceptibility tends to infinity. This means that M has a finite value when B_0 is zero which is an evidence of spontaneous magnetization

From the quantum theory of paramagnetism we can write the equation for spontaneous magnetization as

$$M = Ng\mu_B JB_J(y) \quad \dots\dots\dots(3.4)$$

where $y = \frac{g\mu_B JB}{k_B T} \quad \dots\dots\dots(3.5)$

and $B_J(y)$ is the Brillouin function defined by

$$B_J(y) = \left(\frac{2J+1}{2J}\right) \coth\left[\frac{(2J+1)}{2J}y\right] - \frac{1}{2J} \coth\left(\frac{y}{2J}\right) \quad \dots\dots\dots(3.6)$$

Thus eq. (3.4) can be written as

$$\begin{aligned} M &= Ng\mu_B JB_J \left[\frac{Ng\mu_B J}{Nk_B T} (B_0 + \lambda M) \right] \\ &= M_s(0) B_J \left[\frac{M_s(0)}{Nk_B T} (B_0 + \lambda M) \right] \quad \dots\dots\dots(3.7) \end{aligned}$$

where $M_s(0) = Ng\mu_B J$ represents the maximum value of magnetization at 0K. When there is no magnetic field, $B_0 = 0$ and we get

$$M = M_s(0) B_J \left[\frac{M_s(0)}{Nk_B T} \lambda M \right] = M_s(0) B_J(y) \quad \dots\dots\dots(3.8)$$

where y is given by eq (3.5), in case of ferromagnetic materials, as

$$y = \frac{g\mu_B J}{k_B T} B = \frac{g\mu_B J}{k_B T} (B_0 + \lambda M) \quad \dots\dots(3.9)$$

In case of no magnetic field, $B_0 = 0$ and hence

$$M = \frac{k_B T y}{g\mu_B J \lambda} \quad \dots\dots(3.10)$$

Since M satisfies both eq.(3.8) and eq.(3.10), the two M versus y curves are plotted in Fig. 3.1. Eq (3.10) is a straight line between M and y and for various temperatures i.e. $T < T_c$, $T < T_c$, $T = T_c$ and $T > T_c$ is shown in Fig. 3.1. Eq.(3.8) represents a curve which intersects the straight line for $T < T_c$ at point P. This gives a non-vanishing value of M even if the external field $B_0 = 0$. This spontaneous magnetization below the Curie temperature is shown in Fig 3.2 where the magnetization decreases from a saturated value $M = M_s(0)$ at $T = 0$ to zero at $T = T_c$. At $T = T_c$ the straight line given by eq.(3.10) is the tangent to the curve eq.(3.8) at the origin. Thus there is no spontaneous magnetization for $T \geq T_c$.

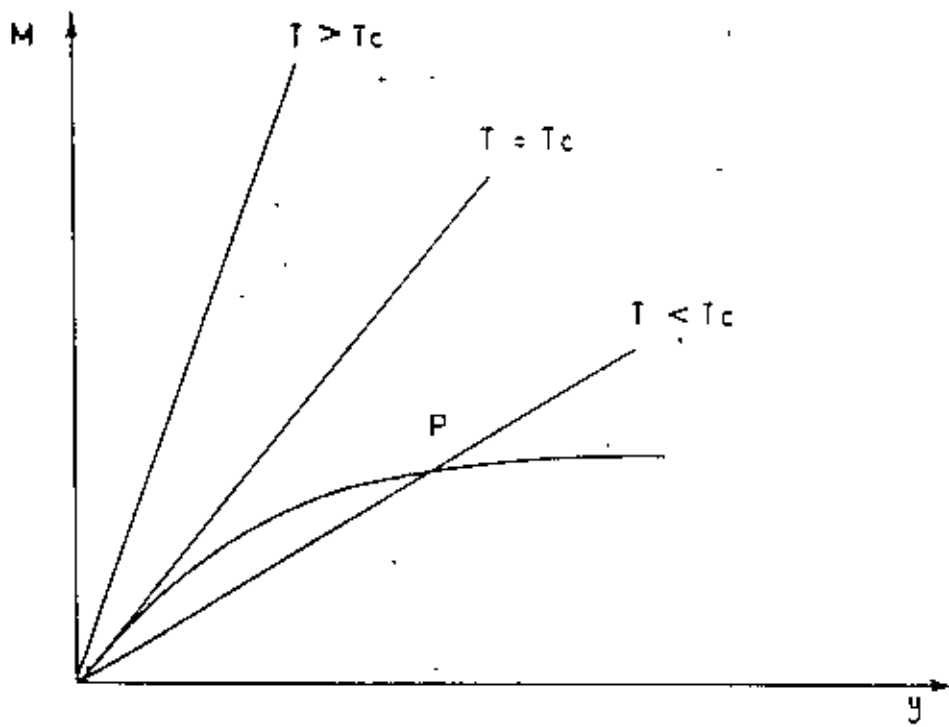


Fig. 3.1 Graphical solution of equations (3.8) and (3.10)

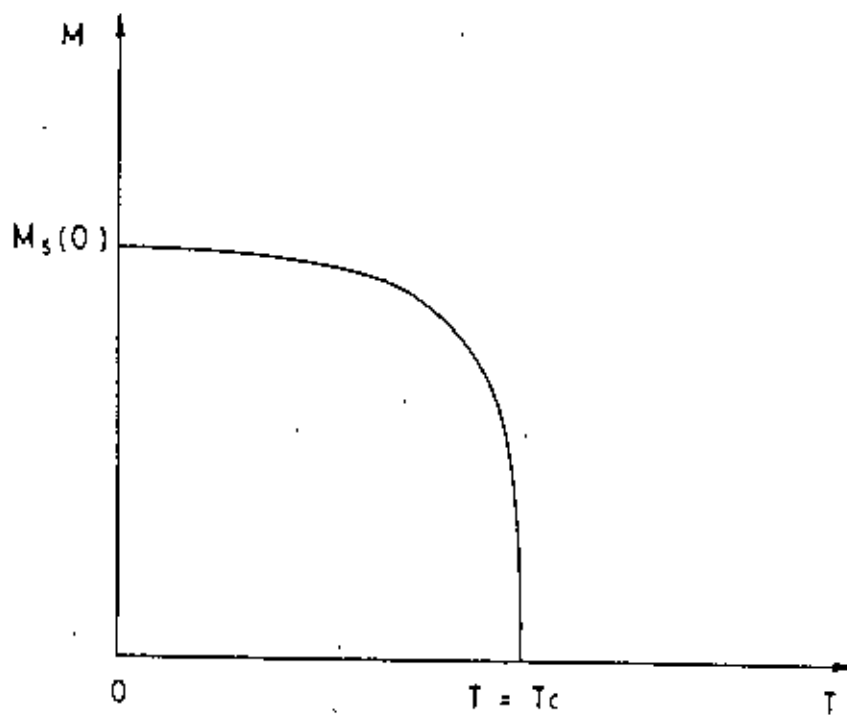


Fig. 3.2 Spontaneous magnetization below the Curie temperature

3.2.1 The molecular field model of ferromagnetism

Most known ferromagnetic substances are metallic. This fact introduces immediately a difficulty which is not really peculiar to magnetism. The problem is the more general one of how to describe the states of motion of the electrons in a metal. When atoms combine to form a metal, their electrons become influenced by the neighbouring atoms. The most tightly bound electrons are hardly affected and remain localised on separate nuclei. The outermost electrons, on the otherhand, are as close to one nucleus as to the next, and they tend to move extensively through the lattice of positive ions, giving the metal its most characteristic property of high electrical conductivity. The magnetic electrons in the ferromagnetic rare earth metals are in $4f$ states and, being screened by the $5s$ and $5p$ electrons, probably remain tightly bound and localised on parent nuclei. In iron, cobalt and nickel, and in their alloys, the electrons responsible for ferromagnetism are those which are derived from the $3d$ states of free ions and are unscreened from neighbouring atoms in a solid sample. They probably exist therefore in states which are itinerant, or at least intermediate between being localised on parent nuclei and being freely itinerant, that is they move through the lattice but their motions are highly correlated as a result of the Coulomb repulsions between them. Such a situation is extremely difficult to analyse theoretically. Molecular field models have been developed for the two limiting cases. The original Weiss model is applicable to electrons which are localised within the positive ions forming the lattice, while the collective-electron model due mainly to Stoner, deals with almost free itinerant electrons.

3.2.2 The localised electron model

Free atoms of iron, nickel and cobalt have $3d$ shells which contain fewer than the maximum $3d$ complement of ten electrons. They possess, therefore, resultant magnetic moments. Similarly, the incompletely populated $4f$ shells of rare earth atoms give rise to resultant moments. The Weiss model is based upon the hypothesis that, when such atoms condense to form metallic solids, the $3d$ or $4f$ electrons retain their localised character, so that ions at the crystal lattice sites constitute the elementary dipoles which are ordered by exchange forces between them.

The ferromagnetic elements like Iron, Cobalt and Nickel and also their alloys are readily magnetised under the influence of an externally applied magnetic field. The degree of spontaneous magnetisation obtaining at a particular temperature is to be determined as a balance between the ordering influence of the molecular field and the disordering effect of thermal agitation. The molecular field representation of the exchange forces makes it possible to investigate the spontaneous magnetisation as a development of statistical theory of paramagnetism. So there is a relation between the intensity of magnetisation M of a paramagnetic sample and the applied field H which induces it. It is

$$M = M_s B_J \left(\frac{\mu_m H}{kT} \right) \quad \dots\dots(3.11)$$

M_s is the saturation magnetisation which would be attained in an infinite field with all the dipoles of moment μ_m aligned, k is Boltzmann's constant, T the absolute temperature and $B_J \left(\frac{\mu_m H}{kT} \right)$ is the Brillouin function of the variable $\frac{\mu_m H}{kT}$ i.e.,

$$B_J(x) = \frac{2J+1}{2J} \coth \frac{2J+1}{2J} x - \frac{1}{2J} \coth \frac{1}{2J} x \quad \dots\dots(3.12)$$

Where J is the angular momentum quantum number of the ions, in terms of which $\mu_m = gJ\mu_B$. When, $J = \frac{1}{2}$ as it does for the spin dipole moment of a single uncompensated electron, the Brillouin function reduces to

$$B_{\frac{1}{2}}\left(\frac{\mu_m H}{kT}\right) = \tanh\left(\frac{\mu_m H}{kT}\right) \quad \dots\dots(3.13)$$

The exchange forces are introduced through the hypothesis that the field acting on each ionic dipole is

$$H = H_a + \gamma M \quad \dots\dots(3.14)$$

Where H_a is the applied field and γM is the molecular field, being proportional to the magnetisation M , with γ the molecular field constant. It has been stressed that the molecular field in a ferromagnetic body is normally very much greater than any other realisable applied field. Neglecting H_a , therefore, we obtain from eq.(3.11)

$$\frac{M_{spont}}{M_s} = B_{\frac{1}{2}}\left(\frac{\mu_m \gamma M_{spont}}{kT}\right) \quad \dots\dots(3.15)$$

The magnetisation here is now the spontaneous magnetisation due to the molecular field, and for this we have used the symbol M_{spont} . Equating eq.(3.15) states how M_{spont} depends on temperature, but M_{spont} appears both sides of the eq.(3.15). It is not possible to rearrange the terms to display M_{spont} as a simple function of T . Instead the variation may be derived graphically by plotting both sides of eq (3.15) against $\frac{\mu_m \gamma M_{spont}}{kT}$, and finding the points at which the curves intersect. Thus in Fig. 3.3 for the right hand side of eq.(3.15), we have the Brillouin function and for the left hand side, $\frac{M_{spont}}{M_s}$ has been drawn as a function of $\frac{\mu_m \gamma M_{spont}}{kT}$

i.e.,
$$\frac{M_{\text{spont}}}{M_s} = \left(\frac{kT}{\mu_m \gamma M_s} \right) \left(\frac{\mu_m \gamma M_s}{kT} \right) \dots\dots(3.16)$$

resulting in a straight line of slope proportional to T . The simultaneous solutions are indicated by the points of coincidence of the two curves at 0 and X. The point 0, corresponding to zero spontaneous magnetisation, would be an unstable equilibrium and the value of M_{spont} at the cross-over point X is the one which would obtain. The variation of M_{spont} with temperature is revealed when the change in slope of the straight line for $\frac{M_{\text{spont}}}{M_s}$ is considered. As remarked the slope is proportional to temperature, and therefore M_{spont} at very low temperatures approaches the value M_s , and decreases as the temperature rises. When the temperature is such that the slope of the line is just equal to the initial slope of the curve for B_f , the only point of intersection is at the origin, and at this and higher temperatures the theory indicates that there will be zero spontaneous magnetisation. This critical temperature at which M_{spont} falls to zero is the Curie temperature T_c and its value in terms of the various molecular field parameters follows from the slope of the Brillouin function at the origin which is $\frac{J+1}{3J}$.

Equating this to the slope of the line we obtain

$$\begin{aligned} T_c &= \frac{J+1}{3J} \frac{\gamma}{k} M_s \mu_m = \frac{J+1}{3J} \frac{\gamma}{k} N \mu_m^2 \\ &= \frac{J(J+1)}{3k} \gamma N g^2 \mu_B^2 = \gamma C \end{aligned} \dots\dots(3.17)$$

where N is the number of dipoles per unit volume. Equating (3.15) may therefore be written as

$$\frac{M_{\text{spont}}}{M_s} = B_f \left(\frac{3J}{J+1} \cdot \frac{T_c}{T} \cdot \frac{M_{\text{spont}}}{M_s} \right) \dots\dots(3.18)$$

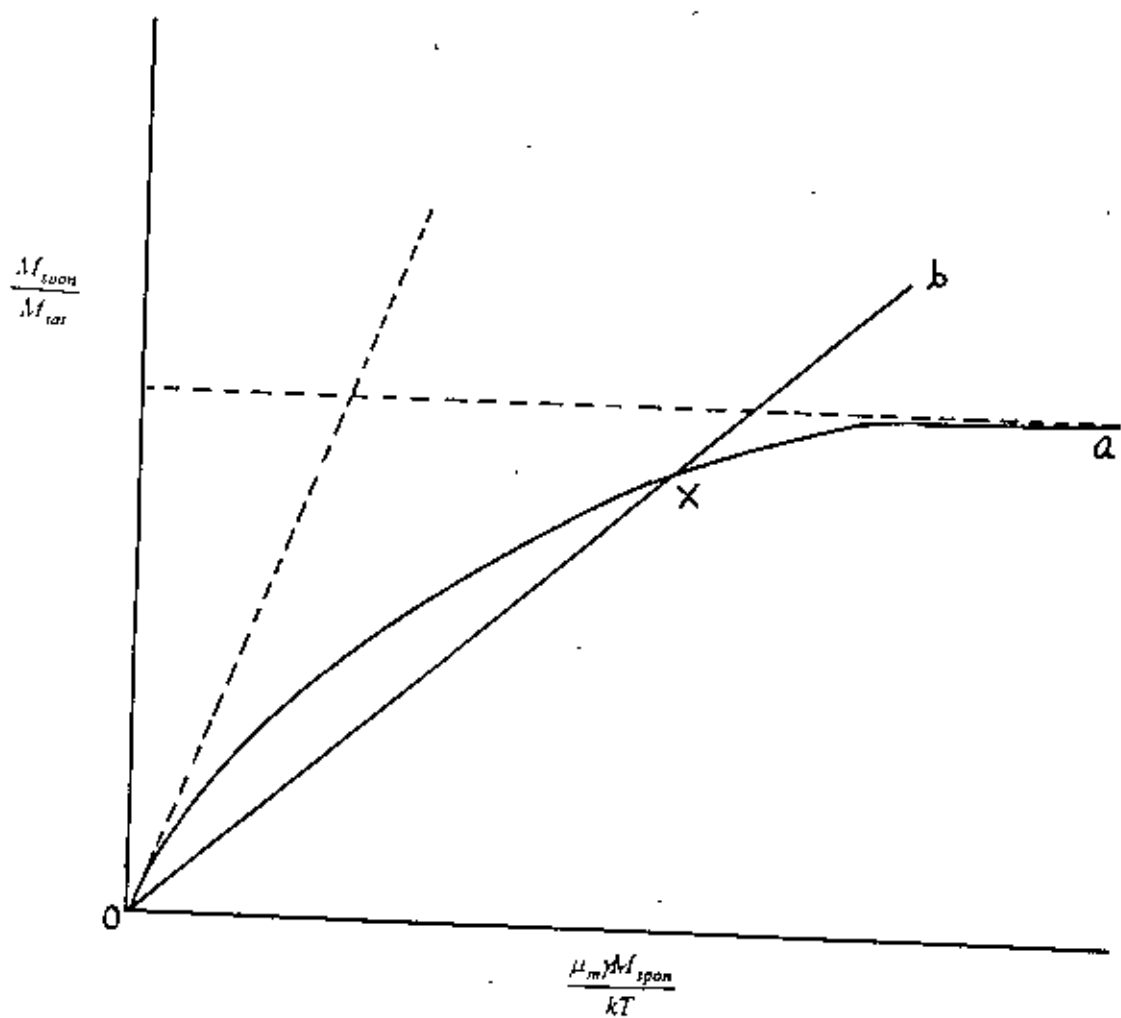


Fig. 3.3 Graphical representation of the spontaneous magnetization of ferromagnetic material

For a given choice of J the variation of $\frac{M_{spin}}{M_s}$ with $\frac{T}{T_c}$ depends only on the form of a Brillouin function and not upon μ_m , γ or N , that is the variation is independent of those parameters which would vary from one material to another. The dependence of the reduced magnetisation $\frac{M_{spin}}{M_s}$ upon the reduced temperature $\frac{T}{T_c}$ is thus a law of corresponding states which, according to the Weiss theory, should be obeyed by all ferromagnetic elements. The physical processes implied by the theory above are, of course, that, as the temperature increases above zero, progressively more dipoles become temporarily excited into disaligned states by the thermal collisions, or fluctuating interactions, between neighbouring atoms until, at $T = T_c$.

3.3 Antiferromagnetism

Heisenberg theory of ferromagnetism is based on the assumption that the exchange integral is positive. When the exchange integral is negative, favouring an anti-parallel orientation of neighbouring spins, we have an antiferromagnetic substance. In an antiferromagnet the spins are ordered in an anti-parallel arrangement with zero net moment at temperatures below the ordering or Néel temperature. Such systems were first investigated theoretically by Néel [36] and Bitter [37]; the theory was later extended by Van Vleck [38], and his formulation is usually regarded as the basic theory of antiferromagnetism. Experimentally, antiferromagnetism was first discovered as a property of MnO by Bizette, Squire, and Tsai in 1938 [39].

Consider a crystal containing two types of atoms A and B distributed over two interlocking lattices. Furthermore, let the interaction between the atoms be such that the A spins tend to line up anti-parallel to the B spins. At low temperatures this

interaction is very effective and in an external field the resulting magnetization will be small. As the temperature is raised, the efficiency of the interaction becomes less pronounced and the susceptibility increases. Finally a critical temperature T_N (the Néel temperature) will be reached above which the spins are “free” and above the temperature the antiferromagnetic material becomes paramagnet, i.e., χ decreases with further increase in T .

An antiferromagnet is a special case of ferrimagnet for which both sublattices A and B have equal saturation magnetizations. Thus $C_A = C_B$, and the Néel temperature in the mean field approximation is given by

$$T_N = \mu C$$

where C_A and C_B are Curie constants for the A and B sites and C refers to a single sublattice. The susceptibility in the paramagnetic region $T > T_N$ can be written as

$$\chi = \frac{2CT - 2\mu C^2}{T^2 - (\mu C)^2} = \frac{2C}{T + \mu C} = \frac{2C}{T + T_N} \quad \dots\dots(3.19)$$

The experimental results at $T > T_N$ are of the form

$$\chi = \frac{2C}{T + \theta} \quad \dots\dots(3.20)$$

Chapter 4

Magnetic Anisotropy

4.1 Theories based on localized electron model

Akulov (1936) is the pioneer to derive the first theoretical expression for the temperature dependence of magnetic anisotropy constant K_1 using a simple classical argument and assuming a system of independent spins. Akulov assumed that each spin has a free energy of the form $K_1 = (\alpha_1^2 \alpha_2^2 + \alpha_2^2 \alpha_3^2 + \alpha_3^2 \alpha_1^2)$, where the direction cosines α_i refer to a particular spin. A simple statistical calculation gives the relationship

$$\frac{K_1(T)}{K_1(0)} \approx \left[\frac{M(T)}{M(0)} \right]^{10} \quad \dots\dots\dots(4.1)$$

between K_1 and the spontaneous magnetization M .

The number 10 arises from the structural combination of the direction cosines in the usual expression for the anisotropy energy; a combination dictated solely by the symmetry of the crystal. The power law holds well for many insulators and rare-earth metals, for which the localized electron model is particularly applicable. But agreement with the experimental data for nickel and iron is not satisfactory; for example, in nickel the temperature variation of K_1 exhibits a dependence of the 50th power of the magnetization (Carr 1958).

In a further classical treatment of magnetic anisotropy Zener (1954), generalised the 10th power law to an $\frac{n}{2}(n+1)$ law assuming a system of independent spins. Zener showed that, if anisotropy energy E_a is written in terms of spherical harmonics,

$$E_a = \sum_n k_n(T) Y_n^m(\alpha) \quad \dots\dots\dots(4.2)$$

then

$$\frac{k_n(T)}{k_n(0)} \approx \left[\frac{M(T)}{M(0)} \right]^{\frac{n}{2(n+1)}} \quad \dots\dots\dots(4.3)$$

Hence the $k_n(T)$ are linear combinations of the $K_l(T)$, and in particular

$$k_2(T) = K_1(T) + \frac{1}{11} K_2(T) + \dots\dots\dots \text{ and } k_3(T) = K_2(T) \quad \dots\dots\dots(4.4)$$

The two assumptions basic to Zener derivation are:

- (i) the existence of regions of short-range order spins around each atom, inside which the anisotropy constants are temperature independent. Thus the only effect of rising the temperature is to introduce small perturbations in the direction of the local magnetization.
- (ii) the distribution of spins within each region is random so that the local anisotropy energy may be averaged over all directions.

The basis for a quantum theory of magnetic anisotropy was laid by Van Vleck (1937) in a paper of anisotropy in metals using the localized electron model. Van Vleck's approach is based on anisotropic contribution to the exchange energy, which appears when the spin-orbit interaction is considered as a perturbation. The second order term is of the same form as a classical dipole-dipole interaction energy, and the fourth order term appears as quadrupole-quadrupole interaction. These two terms provide two models for magnetic anisotropy. The pseudo-dipolar model applied to cubic crystal predicts that anisotropy will vanish if all the dipoles are parallel; quantum mechanically this does not occur, even at 0K. The pseudo-quadrupolar model requires that the spin quantum number be greater than $\frac{1}{2}$, which is unlikely in nickel. Van Vleck used a

Weiss molecular field to portray the exchange interactions. The results of his calculations on each of the two models are as follows:

(a) Dipolar model:

K_1 is of the order of $10^4 J / m^3$, negative for f.c.c. and positive for b.c.c. crystals. This is in agreement with the experimental data for nickel and iron. The temperature variation of K_1 should be according to the square of magnetization.

(b) Quadrupolar model:

K_1 for nickel is of the correct order of magnitude, but the sign is indeterminate. The temperature dependence is as a 5th or 6th power of magnetization. From dimensional consideration K_2 should be about 10^{-3} to 10^{-2} times as great as K_1 . For nickel the experimental value of K_2 is found to be of the same order as K_1 .

The use of a molecular field by Van Vleck assumed no correlation between neighbouring spins. Keffer (1955) replaced the molecular field by a cluster theory, which restored the spin correlation. With this modification, Van Vleck's theory gives the temperature dependence of K_1 as the 10th power of the magnetization at very low temperatures, changing to 6th power at temperatures where the spin correlations are disrupted.

More improved calculations than Van Vleck's, using spin wave theory (Keffer, 1955; Turov and Mitsek, 1959) give the same $\frac{n}{2}(n+1)$ power dependence for the temperature variation of anisotropy. In these cases the anisotropy energy must be written in terms of spherical harmonics, and so the anisotropy constants appearing in the theory are linear combinations of the usual constants.

The use of a molecular field theory can, in fact, give a tenth power law for the temperature variation of K_1 , as was shown by Carr (1958). By expressing the anisotropy energy in terms of Coulomb energy only, Carr (1957) concluded one of the principle mechanisms of anisotropy to be different from those discussed by Van Vleck. Carr obtained the anisotropy constants in terms of electric multipole moments and

crystalline potential constants. The electric multipole moments arise from the spin-orbit coupling inducing an orbital moment. Interaction between the orbital moment and the lattice crystalline potential provides a coupling the spin and the charge distribution. Anisotropy results from distortion of the charge distribution which may occur in a sufficiently inhomogeneous crystalline potential. Carr's theory gives reasonable values of K_1 and K_2 , and it appears that in nickel and cobalt the dominant part of K_1 comes from the interaction of the charge distribution with the crystalline field.

4.2 Pair model of magnetic anisotropy

The physical mechanisms responsible for magnetic anisotropy are dipole-dipole, crystal field or single ion, and anisotropic exchange interactions. Starting from this approaches different calculations have been performed to determine the magnitude, sign and temperature dependence of anisotropy constants.

Magnetic anisotropy describes the circumstance that the energy of a system changes with a rotation of magnetization. The relation between the change in energy of a system with the change in energy of atomic pairs is called the pair model of anisotropy. Van Vleck (1937) first developed this theory. The most important interaction between the atomic magnetic moments is the exchange interaction. This energy is only dependent on the angle between the neighbouring atomic moments, independently of their orientation relative to their bond direction. In a view to explain magnetic anisotropy we may assume that the pair energy is dependent on the direction of the magnetic moment, ϕ as measured from the bond direction. In general we express the pair energy by expanding it in Legendre polynomials;

$$w(\cos\phi) = g + I\left(\cos^2\phi - \frac{1}{3}\right) + g\left(\cos^4\phi - \frac{6}{7}\cos^2\phi + \frac{3}{15}\right) \dots\dots\dots(4.5)$$

The first term is independent of ϕ ; hence the exchange energy is to be included in this terms. The second term is called the dipole-dipole interaction term.

If the pair energy were due exclusively to magnetic dipolar interaction, it should follow that

$$I = -\frac{3M^2}{4\pi\mu_0 r^3} \dots\dots\dots(4.6)$$

The actual of I can be evaluated from the uniaxial crystal anisotropy. In most cases the estimated value is 10^2 to 10^3 times larger than that given by eq.(4.6). The origin of this strong interaction is believed to be the combined effect of spin-orbit interaction and exchange or Coulomb interaction between the neighbouring orbits. That is if there are small amounts of orbital magnetic moment remaining unquenched by the crystalline field, a part of the orbit will rotate with a rotation of the spin magnetic moment because of a magnetic interaction between the two, and the rotation of the orbit will, in turn, change the overlap of the wave functions between the two atoms, giving rise to a change in the electrostatic or exchange energy. This type of interaction is termed as the anisotropic exchange. It should be noted here that the dipolar term of eq.(4.5) does not contribute to the interaction energy E_a since the spins are perfectly parallel. The dipole terms between the atomic pairs with different bond directions cancel out as long as their distribution maintains cubic symmetry. If, however, the crystal has a lower symmetry than the cubic crystal, as in a hexagonal crystal, the dipole-dipole interaction gives rise to magnetic anisotropy.

Van Vleck pointed out that the dipole-dipole interaction does not give rise to cubic anisotropy since the perfect parallelism of the spin system is disturbed by the dipolar interaction itself. Thus if $I < 0$ and all the spins are parallel, the dipole-dipole interaction gives rise to a large pair energy for $\phi = \frac{\pi}{2}$. In such case, a more stable

configuration of the spin pair will be an anti parallel alignment. Some of the spins will therefore take the anti parallel direction in an equilibrium state.

According to Van Vleck's calculation, the cubic anisotropy constants for an f.c.c. system due to dipole-dipole interaction are

$$K_1 = -\frac{9NI^2}{8SMH_m} \quad \text{at } T = 0^\circ K \quad \dots\dots\dots(4.7)$$

where S is the total spin quantum number, M the atomic magnetic moment, and H_m the molecular field. In the classical picture, K_1 should vanish by letting $S \rightarrow \infty$.

Now, since $NMH_m \approx 10^9 J/m^3$ and $NI \approx 10^7 J/m^3$, the order of magnitude of K_1 due to dipole-dipole interaction is

$$K_1 \approx \frac{(NI)^2}{NMH_m} \approx \frac{(10^7)^2}{10^9} \approx 10^5 J/m^3 \quad \dots\dots\dots(4.8)$$

This is sufficient to explain the magnitude of the observed anisotropy energy.

Judging from the origin of anisotropy, it would be practical to suppose that the anisotropy constant decreases with increasing temperature and disappears at the Curie point. Actually this does happen, and the temperature is more drastic than that of spontaneous magnetization. Zener treated this problem in a simple way and explained the temperature dependence fairly well. He assumed that the pair energy is given by eq (4.5) even for the thermally perturbed spin system, since the neighbouring spins maintain an approximately parallel alignment upto the Curie point, where, because of the exchange interaction, parallel spins clusters prevail in the spin system.

Carr followed this method to calculate the crystal anisotropy constant for iron, nickel and cobalt.

Let $(\alpha_1, \alpha_2, \alpha_3)$ denote the direction cosines of the average magnetization, and $(\beta_1, \beta_2, \beta_3)$ are the direction cosines of the local magnetization. Since we assume local

parallelism in the spin system, the anisotropy energy should be given by the average of the local anisotropy energies, so that

$$E_a(T) = K_1(0) \langle \beta_1^2 \beta_2^2 + \beta_2^2 \beta_3^2 + \beta_3^2 \beta_1^2 \rangle \quad \dots\dots\dots(4.9)$$

where $K_1(0)$ is the anisotropy constant at $T = 0^\circ K$ and $\langle \rangle$ denotes the average over all possible orientations of local magnetization. Using the polar co-ordinate (θ, ϕ) , where θ is the angle between the local spin and the average magnetization, and ϕ the azimuthal angle around the magnetization direction. Thus,

$$E_a(T) = K_1(0) \frac{\int_0^\pi \left[\left(\frac{1}{2\pi} \right) \int_0^{2\pi} (\beta_1^2 \beta_2^2 + \beta_2^2 \beta_3^2 + \beta_3^2 \beta_1^2) n(\theta) d\phi \right] n(\theta) d\theta}{\int_0^\pi n(\theta) d\theta} \quad \dots\dots\dots(4.10)$$

where $n(\theta)d\theta$ is the number of spins which point in the solid angle between θ and $(\theta + d\theta)$.

Since

$$\frac{1}{2\pi} \int_0^{2\pi} (\beta_1^2 \beta_2^2 + \beta_2^2 \beta_3^2 + \beta_3^2 \beta_1^2) = \frac{1}{5} [1 - P_4(\cos \theta)] + P(\cos \theta) (\alpha_1^2 \alpha_2^2 + \alpha_2^2 \alpha_3^2 + \alpha_3^2 \alpha_1^2) \dots\dots\dots(4.11)$$

where $P_4(\cos \theta)$ is the fourth order Legendre polynomial. Thus eq.(4.10) becomes

$$E_a(T) = K_1(0) \langle P_4(\cos \theta) \rangle (\alpha_1^2 \alpha_2^2 + \alpha_2^2 \alpha_3^2 + \alpha_3^2 \alpha_1^2) \quad \dots\dots\dots(4.12)$$

where

$$\langle P_4(\cos \theta) \rangle = \frac{\int_0^\pi P_4(\cos \theta) n(\theta) d\theta}{\int_0^\pi n(\theta) d\theta} \quad \dots\dots(4.13)$$

This can be expressed in a polynomial series in

$$\frac{1}{\alpha} = \frac{kT}{MH_m} \quad \dots\dots(4.14)$$

where H_m is the molecular field.

$$\langle P_4(\cos \theta) \rangle = 1 - \frac{10}{\alpha} + \frac{45}{\alpha^2} - \frac{105}{\alpha^3} + \dots\dots \quad \dots\dots(4.15)$$

On the other hand

$$M(T) = M(0) \left(\coth \alpha - \frac{1}{\alpha} \right) \approx M(0) \left(1 - \frac{1}{\alpha} \right) \quad \dots\dots(4.16)$$

so that

$$\left[\frac{M(T)}{M(0)} \right]^{10} \approx 1 - \frac{10}{\alpha} + \frac{45}{\alpha^2} - \frac{120}{\alpha^3} + \dots\dots \quad \dots\dots(4.17)$$

Comparing eq.(4.15) and (4.17) we get

$$\left[\frac{K_1(T)}{K_1(0)} \right] = \left[\frac{M(T)}{M(0)} \right]^{10} \quad \dots\dots(4.18)$$

Relation (4.18) holds good for the temperature dependence of K_1 of iron. Carr also explained the temperature dependence of K_1 for nickel and cobalt by taking into consideration the effect of thermal expansion of the crystal lattice. But, in contrast to

Zener's theory, Van Vleck obtained a much more gentle temperature dependence of magnetic anisotropy. Keffer investigated this point and showed that the Zener's theory is valid at least at low temperature, while Van Vleck's theory is valid at high temperature

4.3 Single-ion model of magnetic anisotropy:

The orbital state of magnetic ions plays an important role in determining magnetic anisotropy. In order to discuss the phenomenon, we must first learn how the orbital state of a magnetic ion is influenced by a given crystalline field and how the resultant orbital states gives rise to magnetic anisotropy. This phenomenon is described by the single-ion model of magnetic anisotropy. This model has been successful in interpreting the magnetic anisotropy of various anti-ferromagnetic and ferromagnetic crystals.

In free atomic states, every $3d$ electronic state has the same energy; in other words their energy levels are degenerate. When the atom is placed in a cubic field, the orbital states of $3d$ electrons are split into two groups. One is the triply degenerate $d\varepsilon$ orbits the special distributions of which are expressed by xy , yz or zx . The other is the doubly degenerate $d\gamma$ orbits whose distributions are expressed by $2z^2 - x^2 - y^2$ and $x^2 - y^2$. Fig. 4.1 explains that the $d\varepsilon$ orbits extend to $\langle 110 \rangle$ directions, while the $d\gamma$ orbits extend along the co-ordinate axes. In octahedral sites, the surrounding anions are found on the three co-ordinate axis, so the $d\gamma$ orbits, which extend towards the anions, have a much higher energy than $d\varepsilon$ orbits because of the electrostatic repulsion between anions and d orbits. For tetrahedral sites $d\gamma$ orbits are more stable than $d\varepsilon$ orbits (Fig. 4.2).

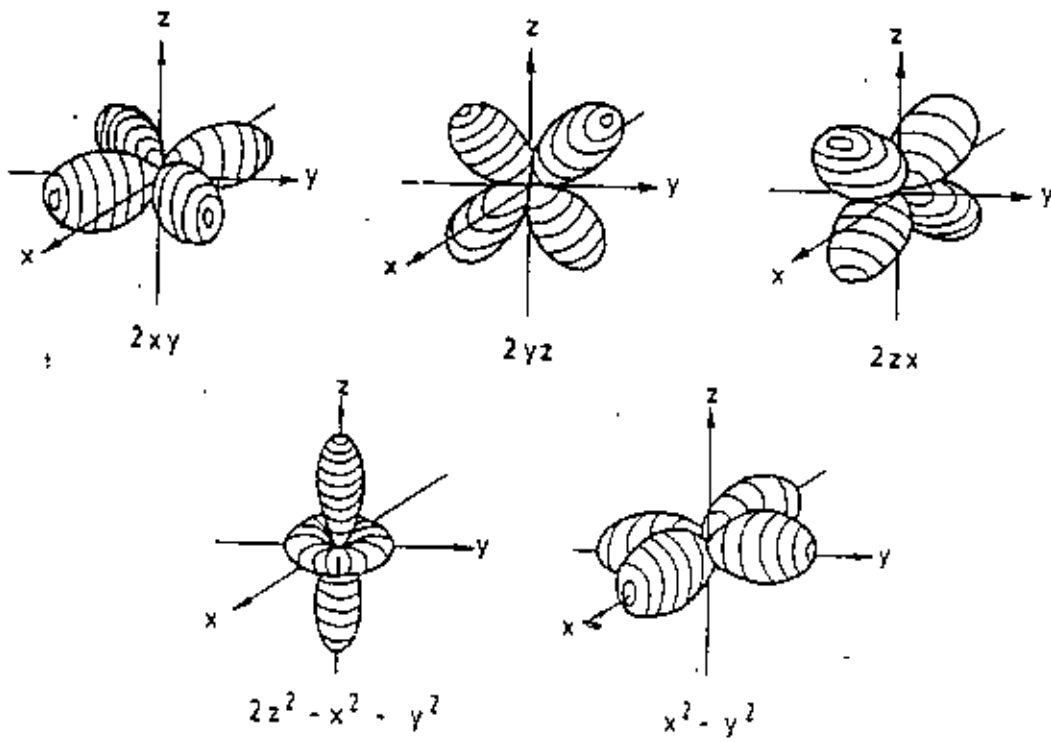


Fig. 4.1 Spatial distribution of d_x and d_y orbitals

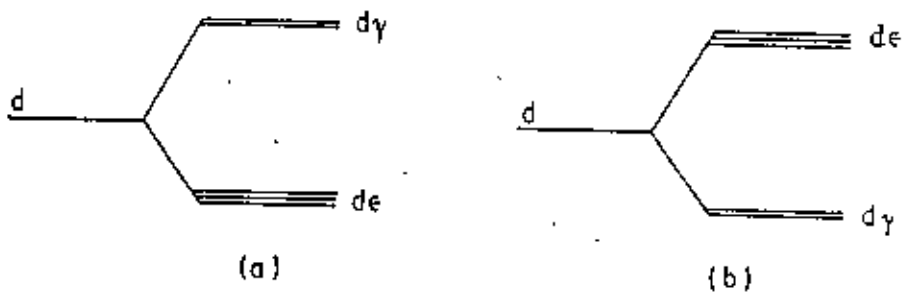


Fig. 4.2 Energy level of d_x and d_y electrons in (a) octahedral and (b) tetrahedral sites

Let us consider the case of the d electrons occupying the $3d$ energy levels. First let us assume that the magnetic ion has only one $3d$ electron. This electron will naturally occupy the lowest energy level. Now as the three $d\varepsilon$ levels have the same energy, the lowest orbital state is triply degenerate (triplet). Such an orbital degeneracy plays an important role in determining the magnetic anisotropy. If there are additional $3d$ electrons, they should occupy exclusively the plus spin levels, because the exchange interaction between these $3d$ electrons is much larger than the energy separation between the dy and $d\varepsilon$ levels. In the case of $(3d)^3$, the three electrons occupy the three $d\varepsilon$ levels, so that the ground state is non-degenerate (singlet). For $(3d^4)$, three electrons occupy the three $d\varepsilon$ levels and remaining one occupies one of the two dy levels, thus the state is doubly degenerate (doublet). In the case of $(3d)^5$, all electrons occupy plus spin levels, so that the ground state is singlet. When there are more than five electrons, the first five fill up the plus spin levels while the remaining electrons occupy the minus spin levels in the same way as for the plus spin levels.

As for the Fe^{2+} ion, the sixth electron should occupy the lowest singlet state, so that the ground state is non-degenerate. On the otherhand, the Co^{2+} ion has seven electrons, so that the last one should occupy the doublet. In such a case the orbit has the freedom to change its state in the plane which is normal to the trigonal axis, so that it has an angular momentum parallel to the trigonal axis. Now since the angular momentum is fixed in direction, it tends to align the spin magnetic moment parallel to the trigonal axis through the spin-orbit interaction. The energy of this interaction can be expressed as $-\lambda LS|\cos\theta|$, where λ is the spin-orbit parameter, L and S are the orbital and spin-angular momentum and θ is the angle between the magnetization and the trigonal axis. This model was first proposed by Slonczewski, who explained the magnetic annealing effect in Co ferrite by this model. He also explained the temperature dependence of the anisotropy constant of cobalt-substituted magnetite. In the normal, or non-magnetically annealed state, Co^{2+} ions should be distributed equally among the four kinds of octahedral sites each of which has its trigonal axis parallel to

one of the four $\langle 111 \rangle$ directions, so that the cubic anisotropy can be obtained by averaging the anisotropy energy $-\lambda L S |\cos \theta|$ over four directions of trigonal axes.

If the ground orbital state is non-degenerate, we cannot expect any orbital angular momentum so long as the atom stays in the ground state; in other words, the orbital angular momentum is quenched by the crystalline field. In such a case we cannot expect an anisotropy as large as that of the Co^{2+} ion in an octahedral site. There are, however, various sources which result in a fairly small magnetic anisotropy, which is nevertheless sufficiently large to account for the observed values. Yosida and Tachiki calculated the various types of anisotropy and applied their results to the *Mn*, *Fe* and *Ni* ferrites, which contain Mn^{2+} , Fe^{3+} , Fe^{2+} and Ni^{2+} ions. Firstly they found that the magnetic dipole-dipole interaction is too weak to account for the observed magnitude of anisotropy. The main source of anisotropy is thought to be the distortion of the $3d$ shell from spherical symmetry. In a distorted $3d$ shell the inter-atomic dipole-dipole interaction between the spin magnetic moments may depend on the direction of magnetization; this is similar to the dependence of the magneto static energy on the direction of magnetization in a fine elongated single domain particle, and gives rise to the anisotropy energy.

The anisotropy is also induced through spin-orbit interaction. That is, some amount of orbital angular momentum can be induced by spin-orbit interaction by exciting additional orbital states. In a distorted $3d$ shell this excitation is dependent on the direction of magnetization, giving rise to anisotropy. Yosida and Tachiki showed that the anisotropy due to these mechanisms should vanish for $S = \frac{1}{2}$, 1, and $\frac{3}{2}$, where S is the total spin angular momentum, and the anisotropy of this type cannot be expected for Ni^{2+} and Co^{2+} ions. Accordingly, the main source of the anisotropy of *Mn*, *Fe* and *Ni Mn* ferrites is considered to be the Mn^{2+} , Fe^{3+} , and Fe^{2+} ions. Since Ni^{2+} ion has no effect on the magnetic anisotropy in *Ni* ferrite, the difference in anisotropy energy between *Fe* and *Ni* ferrites must be explained by the anisotropy due to Fe^{2+}

ions. Yosida and Tachiki also calculated the temperature dependence of the anisotropy constant for *Mn* ferrites and fitted the theory with experiment.

4.4 Physical origin of magnetocrystalline anisotropy

Phenomenologically magnetic anisotropy of a ferromagnetic single crystal is usually expressed in terms of free energy E_a , which is assumed to be a function of the direction cosines α_1 , α_2 and α_3 of the magnetization vector M with respect to crystallographic axes. Considering cubic symmetry and the fact that the total Hamiltonian of a given system is invariant under the time reversal transformation in the absence of an external magnetic field, we can write

$$E_a = K_0 + (\alpha_1^2 \alpha_2^2 + \alpha_2^2 \alpha_3^2 + \alpha_3^2 \alpha_1^2) + K_2 (\alpha_1^2 \alpha_2^2 \alpha_3^2) + \dots \quad \dots \dots (4.19)$$

for a cubic crystal.

For a crystal of uniaxial anisotropy the corresponding equation is

$$E_a = K_{a1} \sin^2 \varphi + K_{a2} \sin^4 \varphi \quad \dots \dots (4.20)$$

Where φ is the angle between the axis of easy magnetization and the direction of magnetization vector.

Crystal anisotropy originates mainly from the spin-orbit coupling. By coupling is meant a kind of interaction which keeps the moments either parallel or anti parallel to each other. Crystal anisotropy may be regarded as a force which tends to bind the magnetization to directions of a certain form in the crystal. Thus we could speak of the

exchange interaction between two neighbouring spins parallel or anti parallel to one another. But the associated exchange energy is isotropic and it depends only on the angle between the adjacent spins, but not on the direction of the spin axis relative to the crystal lattice. The spin-spin coupling therefore cannot contribute to the crystal anisotropy. The orbit-lattice coupling is also strong. This follows from the fact that orbital magnetic moments are almost entirely quenched. This means, in effect, that the orientations of the orbits are fixed very strongly to the lattice, because even large fields cannot change them.

There is also a coupling between the spins and the orbital motion of the electrons when the orbital angular momentum remains partially unquenched. When an external field tries to reorient the spin of an electron, the orbit of that electron also tends to be reoriented. But the orbit is strongly coupled to the lattice and therefore resists the attempt to rotate the spin axis. The energy required to rotate the spin system of a domain away from the easy direction, which we call the anisotropy energy, is just the energy required to overcome the spin-orbit coupling. This coupling is relatively weak because fields of a few hundred gauss are usually strong enough to rotate the spins. Inasmuch as the lattice is really constituted by a number of atomic nuclei arranged in space, each with its surrounding cloud of orbital electrons, we can also speak of a spin lattice coupling and conclude that it too is weak. The strength of anisotropy in any particular crystal is measured by the magnitude of the anisotropy constants K_1 , K_2 , etc. although there is no doubt that crystal anisotropy is due to spin-orbit coupling, the details are different, and it not possible to calculate the value of the anisotropy constants from the first principles.

As the theory of ferromagnetism in nickel and other $3d$ metals is still not understood fully, the origin of magnetic anisotropy in these materials remain, to a considerable extent, phenomenological. Brief review of theories follow that the attempts to explain the temperature dependence of magnetic anisotropy have completely dominated the minds of the theoreticians. However the problem of producing a theory of the temperature dependence of magnetic anisotropy in $3d$ metals is enormous.

The anisotropy energy depends on the direction of magnetization relative to the crystal lattice. Thus their magnetic moments must be coupled to the crystal in some manner. In the iron-group ferromagnetic materials the magnetic moments, due to spin moments of the $3d$ electrons are coupled indirectly to the lattice via spin-orbit and orbit lattice couplings. The extent of the influence of lattice symmetry on a magnetic ion will depend strongly on its electronic structure.

In rare-earth metals and compounds, on the otherhand, the magnetic moments consist of both spin and orbital contributions because of the strong spin-orbit coupling. The magnetic anisotropy therefore arises from a direct orbital-lattice coupling.

The $3d$ electrons responsible for the magnetic moments in iron group ionic crystals are well localized about each lattice site, so that it is possible to treat the disturbing effects of surroundings as small perturbations on a free-ion state. Thus the magnetic anisotropy can be calculated on the basis of Van Vleck's theory.

In $3d$ metals and alloys, the orbital moments are quenched by a mechanism which differs somewhat from that in insulators; this is due to electron transfer or hopping. Nevertheless magnetic anisotropy is caused by orbital moments induced by spin-orbit coupling, and the mechanism for anisotropy must be essentially the same as in insulators. For this reason, theories based on localized electron model (Van Vleck, 1937; Zener, 1954 and others) provide a qualitative understanding of magnetic anisotropy.

The observed temperature variation of the anisotropy constants of metals such as nickel is very rapid. On the other hand, the magnetostrictive energy the origin of which is the spin-orbit coupling shows a very much slower variation with temperature. Thus according to Zener (1954), the decrease in the anisotropy constant with increasing temperature cannot be due to a weakening of the spin-orbit coupling.

The $3d$ shells of $3d$ transition metals and alloys are the most exposed except for the $4s$ conduction electrons. The energy levels of these electrons, responsible for ferromagnetism, is perturbed due to overlapping of the $3d$ shells of neighbouring atoms. This perturbation gives rise to a spread in the energy levels of $3d$ electrons to

form an energy band. The description of magnetic anisotropy and magnetostriction cannot therefore be obtained in the strict sense on the basis of localized electron model which has relatively more success for insulators and rare-earth metals. On the other hand, the description of these phenomena in the band theory of ferromagnetism in terms of the effects of crystalline field and spin-orbit interaction as attempted by Fletcher and Katayama becomes inexact due to difficulty of treating different electron spin correlation functions correctly.

4.5 The temperature dependence of magnetocrystalline anisotropy

The temperature dependence of magnetocrystalline anisotropy is established by theoretical arguments with increasing generality (Callen and Callen 1966) to follow the general $\frac{n}{2}(n+1)$ power law, i.e.,

$$\frac{K(T)}{K(0)} = \left[\frac{M(T)}{M(0)} \right]^{2^{(n+1)}} \quad \dots (4.21)$$

Where $K(0)$ is the anisotropy constants at $0^\circ K$ and $K(T)$ is the anisotropy constant at $T^\circ K$. $M(0)$ is the magnetization at $0^\circ K$ and $M(T)$ is the magnetization at $T^\circ K$. The $\frac{n}{2}(n+1)$ power law of the temperature dependence of the magnetocrystalline anisotropy at low temperature is derived in general fashion by Callen and Callen (1966). The problem of temperature dependence of anisotropy energy takes its beginning from the famous tenth power law, formulated for the first time by Akulav. Callen and Callen have reviewed the origin of the tenth power law.

The magnetocrystalline anisotropy is defined in terms of the dependence of free energy on the direction of magnetization. For a cubic ferromagnet the free energy is usually expanded in a power series in the direction cosines $\alpha_1, \alpha_2, \alpha_3$ of the magnetization direction relative to the crystallographic axis. Symmetry dictates that this power series takes the form

$$F = K_0(T) + K_1(T)[\alpha_1^2 \alpha_2^2 + \alpha_2^2 \alpha_3^2 + \alpha_3^2 \alpha_1^2] + K_2(T)\alpha_1^2 \alpha_2^2 \alpha_3^2 \dots \dots \dots (4.22)$$

Akulov showed by a simple classical argument that

$$\frac{K_1(T)}{K_1(0)} \cong 1 - 10\delta m \cong [1 - \delta m]^{10} \cong [m(T)]^{10} \dots \dots \dots (4.23)$$

where $m(T)$ is the reduced magnetization $\left(= \frac{M(T)}{M(0)} \right)$ and where $\delta m(T) = 1 - m(T)$.

The Akulov result applies only at temperatures sufficiently low that $\delta m \ll 1$. The Akulov derivation is based on the assumption of independent classical spins, each of which has an energy of the form of eq (4.22). The power 10 in eq. (4.23) arises not from a particular model but rather from the particular structural combination of the direction cosines in eq. (4.22). This combination is completely dictated by the symmetry of the crystal. Thus the Akulov derivation, did identify the source of the 10th power law. Akulov compared the theoretical result with the data of Honda et al. on iron, and concluded that the law was quite accurately obeyed upto $T \approx 0.65T_c$.

In 1955 Keffer recognized that the paradox posed by the disagreement of Akulov's theorem and Van Vleck's molecular field calculations arose from the violence that molecular field theory does to spin correlations. He therefore recalculated the anisotropy of pseudo-quadrupolar origin, substituting a cluster theory for molecular field theory. This cluster theory has been incidentally introduced by Van Vleck in 1937. This concept was later fully exploited Oguchi. Keffer then found that the pseudo-quadrupolar interaction would give a 10th power law at low temperatures, changing

rapidly to Van Vleck's 6th power dependence as increasing temperature disrupts the spin correlations. Keffer also rederived the Zener $\frac{n}{2}(n+1)$ generalisation, using the classical single-ion mechanism and molecular field theory. At this point it was clear that single ion terms in the Hamiltonian were completely consistent with the $\frac{n}{2}(n+1)$ power law, and Keffer's cluster calculation was generally accepted as establishing the theorem for pseudo-quadrupolar interactions.

Peculiarly in the very paper in which Keffer established the $\frac{n}{2}(n+1)$ law for the single ion and pseudo-quadrupolar terms and identified the critical role of spin correlations. He also briefly remarked that a spin-wave analysis of the dipolar terms would probably give a power even lower than two. Kasuya then carried out just such a spin-wave calculation for the pseudo-dipolar terms and found a 16th power. Charap and Weiss found an error of a factor of 2 in Kasuya's calculation and concluded that the 8th power was correct. Finally Keffer and Oguchi added certain terms omitted by Charap and Weiss, regained the 10th power law in all cases.

In 1959 Turov and Mitsek deduced the $\frac{n}{2}(n+1)$ power dependence from the spin-wave approach of Kasuya. In 1966 Callen and Callen showed that this law can be generalised to higher anisotropy constants of arbitrary crystal symmetry, to a quantum mechanical treatment, to two ion as well as one ion mechanism and to arbitrary temperatures.

The theory predicts that for cubic crystals the anisotropy constants are related to magnetization as,

$$\frac{K_2^0(T)}{K_2^0(0)} = \left[\frac{M(T)}{M(0)} \right]^{10} ; \quad \frac{K_4^0(T)}{K_4^0(0)} = \left[\frac{M(T)}{M(0)} \right]^{21} \quad \dots\dots(4.24)$$

And for hexagonal crystal

$$\frac{K_2^0(T)}{K_2^0(0)} = \left[\frac{M(T)}{M(0)} \right]^3 ; \quad \frac{K_4^0(T)}{K_4^0(0)} = \left[\frac{M(T)}{M(0)} \right]^{10}$$

and

$$\frac{K_6^0(T)}{K_6^0(0)} = \frac{K_6^6(T)}{K_6^6(0)} = \left[\frac{M(T)}{M(0)} \right]^{21} \quad \text{.....(4.25)}$$

When these coefficients are expressed in terms of anisotropy constants K_1, K_2, \dots which are generally measured in the analysis of the torque curve, the expressions (4.22) and (4.23) become

For cubic crystal

$$K_1(T) = \left[K_1(0) + \frac{1}{11} K_2(0) \right] \left[\frac{M(T)}{M(0)} \right]^{10} - \frac{1}{11} K_2(0) \left[\frac{M(T)}{M(0)} \right]^{21} \quad \text{.....(4.26)}$$

$$K_2(T) = K_2(0) \left[\frac{M(T)}{M(0)} \right]^{21} \quad \text{.....(4.27)}$$

For hexagonal crystals

$$K_1(T) = \left[K_1(0) + \frac{8}{7} K_2(0) + \frac{8}{7} K_3(0) \right] \left[\frac{M(T)}{M(0)} \right]^3 - \left[\frac{8}{7} K_2(0) + \frac{144}{77} K_3(0) \right] \left[\frac{M(T)}{M(0)} \right]^{10} + \frac{8}{3} K_3(0) \left[\frac{M(T)}{M(0)} \right]^{21} \quad \text{.....(4.28)}$$

$$K_2(T) = \left[K_2(0) + \frac{18}{11} K_3(0) \right] \left[\frac{M(T)}{M(0)} \right]^{10} - \frac{18}{11} K_3(0) \left[\frac{M(T)}{M(0)} \right]^{21} \quad \text{..... (4.29)}$$

$$K_3(T) = K_3(0) \left[\frac{M(T)}{M(0)} \right]^{21} \quad \text{.....(4.30)}$$

$$K_4(T) = K_4(0) \left[\frac{M(T)}{M(0)} \right]^{21} \quad \text{..... (4.31)}$$

However, neither of the expressions (4.24) or (4.25) is found to be in good agreement with the observed behaviour of the iron group elements. For iron (cubic) $K_1(T)$ varies

as approximately as the sixth power of $\frac{M(T)}{M(0)}$, whilst in nickel the variation is much faster than $\left[\frac{M(T)}{M(0)}\right]^{10}$ and nearly follows $\left[\frac{M(T)}{M(0)}\right]^{20}$ at lower temperature.

From all the model discussed so far, it is evident that the ferromagnetic anisotropy is caused by an anisotropic term in the exchange energy. The anisotropic exchange is caused by the spin-orbit coupling which relates the spin to the dependence of interatomic energy on the orientation of the orbital wave functions. The origins of magnetic anisotropy, mainly with reference to insulators, are reviewed by Yosida (1968), Kanamori (1963) and Callen and Callen (1966).

The $\frac{n}{2}(n+1)$ power law for the temperature dependence of anisotropy constants, in particular the 10th power law for K_1 , obtains in all the theories that can treat the temperature variation of the anisotropy energy. It may be derived quite generally, both quantum mechanically and classically (Van Vleck, 1956). In either case the law is valid at low temperatures only, because classically it is assumed that the spin deviations are small, and quantum mechanically only the ground and the first excited states are occupied.

On the otherhand, it has been found by many workers that a highly satisfactory fit to experimental data is given by the empirical relationship of Bryuchatov and Kirensky (1937),

$$\frac{K_1(T)}{K_1(0)} = \exp(-aT^2) \quad \dots\dots\dots(4.32)$$

which is frequently used to determine $K_1(0)$ by extrapolation. This holds for nickel up to room temperature. A thermodynamic argument has been given in favour of this relationship by Stato and Tono (1956).

The mathematical expression of the behaviour of the anisotropy constants at low temperatures, derived theoretically, is

$$\frac{K_n(0) - K_n(T)}{K_n(0)} = \frac{n}{2}(n+1) \left[\frac{M(0) - M(T)}{M(0)} \right] \quad \dots\dots(4.33)$$

i. e.
$$\frac{K_n(T)}{K_n(0)} = 1 - \frac{n}{2}(n+1)\delta M(T) \quad \dots\dots(4.34)$$

where
$$\delta M(T) = \frac{M(0) - M(T)}{M(0)}$$

Since the anisotropy is assumed to vanish at the Curie temperature the linear expression of eq.(4.28) cannot be exact. Hence it represents the first two terms of a binomial expression,

$$\frac{K_n(T)}{K_n(0)} = [1 - \delta M(T)]^{\frac{n}{2}(n+1)} = \left[\frac{M(T)}{M(0)} \right]^{\frac{n}{2}(n+1)} \quad \dots\dots(4.35)$$

At temperatures sufficiently far from the Curie temperature

$$\frac{K_n(T)}{K_n(0)} = \exp \left[-\frac{n}{2}(n+1)\delta M(0) \right] \quad \dots\dots(4.36)$$

If the temperature variation of the spontaneous magnetization is taken to be

$$\frac{M(T)}{M(0)} = 1 - A \left(\frac{M}{T_c} \right) \quad \dots\dots(4.37)$$

then

$$\frac{K_n(T)}{K_n(0)} = \exp \left[-B \left(\frac{M}{T_c} \right)^m \right] \quad \dots\dots(4.38)$$

where
$$B = \frac{n}{2}(n+1)A$$

From spin wave theory $m = \frac{3}{2}$ at low temperatures and eq.(4.37) has been confirmed to a high accuracy (Pugh Argyle, 1962) for nickel. The derived constant of $\frac{A}{T_c^{\frac{3}{2}}}$ is of

order 4×10^{-6} . It must be admitted that the temperature dependence of $\frac{K_1'(T)}{K_1'(0)}$ for Ni does not follow the expression (4.32) with $m = \frac{3}{2}$, nor the initial slope of a graph of $\log \left[\frac{K_1'(T)}{K_1'(0)} \right]$ in agreement with the predicted value of $\frac{u}{2}(n+1)AT_c^{-\frac{1}{2}}$. However it has been the common experience of many experimentalists that eq.(4.37) does fit experimental magnetization data with $m=2$ over a large temperature range. However none of the theories of anisotropy can explain the change in sign of K_1 of nickel that is found experimentally to occur about $200^\circ C$. A change in sign of K_1 would apparently suggest a change in sign of the magnetization which is incorrect. It is possible if corrected to constant volume K_1 may be found to remain negative.

4.6 Magnetocrystalline anisotropy of Nickel

In nickel the direction of easy magnetization is of the form [111], the body diagonal of the unit cell. It means that saturation can be achieved with quite low field in the [111] direction. But a fairly high field is needed to saturate nickel in a [110] direction. For this orientation of the field, the domain structure changes. The only way in which the magnetization can increase further is by rotation of the M_S vector of each domain until it is parallel with the applied field. Domain rotation occurs only in fairly high fields, because the field is then acting against the force of crystal anisotropy, which is usually fairly strong. So a high field is required to saturate nickel in the [100] direction which is called the hard direction. Because the applied field must do work against the anisotropy force to turn the magnetization vector away from an easy direction, there must be energy stored in nickel in which M_S points in a noneasy direction. This is

called the magnetocrystalline anisotropy energy of nickel. The temperature dependence of magnetocrystalline anisotropy of nickel is also an interesting property. According to Zener the effect of temperature upon magnetocrystalline anisotropy arises solely from the introduction of local deviations in the direction of magnetization. This deviation in an elementary region is the resultant of very large number of independent deviations.

4.7 Different measurement techniques of magnetic anisotropy

4.7.1 Ferromagnetic resonance method

There are several ways to measure the magnetocrystalline anisotropy of a magnetic material. One of the ways is the ferromagnetic resonance. When an alternating magnetic field of high frequency is applied to a magnetic substance, certain resonance effects are observed at particular values of the frequency and magnitude of the field. The effect is one of the two kinds: One involves the magnetic moment of the electron which arises due to the spin of the electron around the nucleus. The electron moment interacts with the applied external a.c magnetic field and precesses when the resonance between the electron spin frequency and the frequency of the applied external field occurs. The other method is to measure the magnetocrystalline anisotropy.

The first effect which is usually due only to electron spin can be observed in ferro-, antiferro-, and ferrimagnetic substances, where the spins are coupled by exchange forces. Here resonance measurements can reveal the crystal anisotropy constant K_1 . When the constant field H is directed parallel to the easy axis of a crystal, two forces act to turn the spins toward the easy axis: the applied external magnetic field H , and the crystal anisotropy, which can be regarded as an anisotropy field H_A . The resonance condition then becomes

$$h\nu = g\mu_B(H + H_K) \quad \dots\dots(4.39)$$

and H_K is related to K_1 by

$$H_K = \frac{2K_1}{M_s} \quad \dots\dots(4.40)$$

If resonance measurements are made parallel to several crystal directions in a cubic crystal, the value of both K_1 and K_2 may be found.

The resonance frequency depends on the effective internal magnetic field which exerts a torque on the precessing spin system. Magnetic anisotropy contributes a torque on a spin system if the spins point in other than the easy or hard directions, thus affecting the resonance frequency. The equation of motion of the magnetization vector is given by

$$\left(\frac{1}{\gamma}\right)\left(\frac{dM}{dt}\right) = M \times H + \text{torque due to anisotropy energy}$$

By calculating the frequency of the small oscillation of M around the equilibrium position one can express the resonance frequency in terms of B and anisotropy constant. γ is the gyro-magnetic ratio.

This method enables measurements of the anisotropy to be made on very small single crystal specimens. It also offers information about the magnitude of the local anisotropy, as distinct from the bulk anisotropy determined by other methods.

4.7.2 Magnetic torque method

Since ferromagnetic crystals have easy and hard directions of magnetization, the energy associated with the magnetization depends on the direction. In order to obtain the anisotropy energy in terms of direction of magnetisation, we make use of the

crystal symmetry. The energy variation with respect to sample orientation is represented by a torque exerted on the sample. When an anisotropic single crystal is suspended in a uniform magnetic field, a torque acts on it tending to align an easy direction of magnetization along the field direction. The torque exerted per unit volume of the specimen is

$$L = -\frac{dE_a}{d\phi} \quad \text{.....(4.41)}$$

where ϕ is the angle of rotation of the easy direction of magnetization, from which the anisotropy constants may be evaluated. This method has the advantage that contributions to the torque from sources other than the magnetic anisotropy can generally be distinguished in the torque curves.

4.7.3 Magnetization method

Another method of measuring the magnetic anisotropy is the measurements of magnetisation along the different crystallographic directions, and calculating the area under the M versus H curves. The area under the M versus H curves is a measure of the anisotropy energy. This energy differs from one crystallographic direction to the other.

The shape of the magnetization curve for a magnetic field applied in a particular crystallographic direction depends on the values of the anisotropy constants. The theoretical expressions for the magnetization in terms of the magnetic field and the anisotropy energy can be calculated, and comparison with experimental values enables the anisotropy constants to be determined.

When a ferromagnetic material is magnetized in an applied magnetic field H , the free energy E_a stored in the system is represented by

$$E_a = \int_0^{M_s} H \cdot dM \quad \dots\dots\dots(4.42)$$

where M_s is the saturation magnetization. The quantity $\int H \cdot dM$ represents the area bounded by the magnetization curve for the direction concerned, by the axis for M and by the line $M = M_s$. Phenomenologically, magnetocrystalline anisotropy of a ferromagnetic single crystal is usually expressed in terms of a free energy E_a which is assumed to be a function of direction cosines α_1, α_2 and α_3 of the magnetization vector M with respect to the crystallographic axes. Considering cubic symmetry and the fact that the total Hamiltonian of a given system is invariant under the time reversal transformation in the absence of an external magnetic field, E_a can be expressed as

$$E_a = K_1(\alpha_1^2\alpha_2^2 + \alpha_2^2\alpha_3^2 + \alpha_3^2\alpha_1^2) + K_2(\alpha_1^2\alpha_2^2\alpha_3^2) \quad \dots\dots\dots(4.43)$$

where α 's are the direction cosines of the magnetization vector with respect to the crystallographic axes and K_1 and K_2 are the first and the second anisotropy constants respectively.

If the energy for the three crystallographic directions are $E_{a_{[111]}}$, $E_{a_{[110]}}$ and $E_{a_{[100]}}$ respectively, then

$$E_{a_{[111]}} - E_{a_{[100]}} = \frac{K_1}{3} + \frac{K_2}{27} \quad \dots\dots\dots(4.44)$$

since $\alpha_1 = \alpha_2 = \alpha_3 = \frac{1}{\sqrt{3}}$ for $[111]$ direction, and $\alpha_2 = \alpha_3 = 0, \alpha_1 = 1$ for $[100]$ direction.

Similarly,

$$E_{a_{[110]}} - E_{a_{[100]}} = \frac{K_1}{4} \quad \text{.....(4.45)}$$

since $\alpha_2 = \alpha_3 = \frac{1}{\sqrt{2}}, \alpha_1 = 0$ for $[110]$ direction.

Thus

$$K_1 = 4 \left(E_{a_{[110]}} - E_{a_{[100]}} \right) \quad \text{.....(4.46)}$$

Chapter 5

Experimental

5.1 The torque measurement

Magneto-crystalline anisotropy and its temperature dependence which are the main aspects of this thesis is determined by Torque Magnetometer. The procedure of measuring torques in the range $10^{-10} Nm$ to $5.10^{-4} Nm$ is described here. Torque compensation is achieved by feedback from a photodetector into a PID regulator system which generates a current through a compensation coil located in the field of permanent magnets. Stability criteria for the regular system are discussed. The apparatus permits continuous measurement of the torque as a function of angle with simultaneous registration of the data on x-y recorder and on paper tape for computer analysis. Measurements can be made in the temperature range $4.2K$ to $800K$

The inherent property of a magnetic material in a static magnetic field is to align itself in order to minimise its energy. The energy variation with respect to sample orientation is represented by a torque exerted on the sample. The torque L exerted along an axis perpendicular to the magnetic field is related to the total anisotropy energy E_a and is given by

$$L = -\frac{dE_a}{d\theta} \quad \dots\dots(5.1)$$

where θ is the angle between a fixed direction in the sample and the direction of the magnetic field. Thus it is evident that by measuring the torque from a sample in a magnetic field we can gain information about the magnetic anisotropy energy of a material. For ferromagnetic substances the anisotropy constants can be deduced from

Fourier analysis of the torque data as a function of the angle θ between the magnetic field and a direction fixed in the crystal.

Akulov (1929) showed that E_a can be expressed in terms of a series expansion of the direction cosines of M_s (saturation magnetization) relative to the crystal axes. In a cubic crystal, let M_s makes angles a, b, c with the crystal axes and let $\alpha_1, \alpha_2, \alpha_3$ be the cosines of these angles, then the anisotropy energy may be written as,

$$E_a = K_0 + K_1(\alpha_1^2\alpha_2^2 + \alpha_2^2\alpha_3^2 + \alpha_3^2\alpha_1^2) + K_2(\alpha_1^2\alpha_2^2\alpha_3^2) \quad \dots\dots\dots(5.2)$$

where K_0, K_1, K_2 are respectively the zero, first and second order anisotropy constants. The first term, which is simply K_0 , is independent of angle and is usually ignored, because normally we are interested only on the change in energy E_a when the M_s vector rotates from one direction to another. When K_2 is zero, the direction of easy magnetization is determined by the sign of K_1 . If K_1 is positive, then $E_{100} < E_{110} < E_{111}$ and then [100] is the direction of easy magnetization. If K_1 is negative then, $E_{111} < E_{110} < E_{100}$ and thus the [111] crystallographic direction is the direction of easy magnetization. For nickel K_1 is negative.

For a specimen cut in a (100) plane for a single crystal of cubic structure, if a strong field H_e is applied at an angle θ to the fixed direction of the sample then the crystal may be magnetized to saturation with the saturation vector M_s . The resultant field H in the specimen is then the vector difference of H_e and the demagnetizing field $N_D M_s$. The anisotropy energy when M_s is at an angle θ to the field direction direction in a (100) plane can be written as

$$E_a = K_0 + \frac{K_1}{8}(1 - \cos 4\theta)$$

The torque on the specimen per unit volume is

$$L = -\frac{dE_a}{d\theta}$$

Therefore,

$$L_{(100)} = -\frac{K_1}{2} \sin 4\theta \quad (5.3)$$

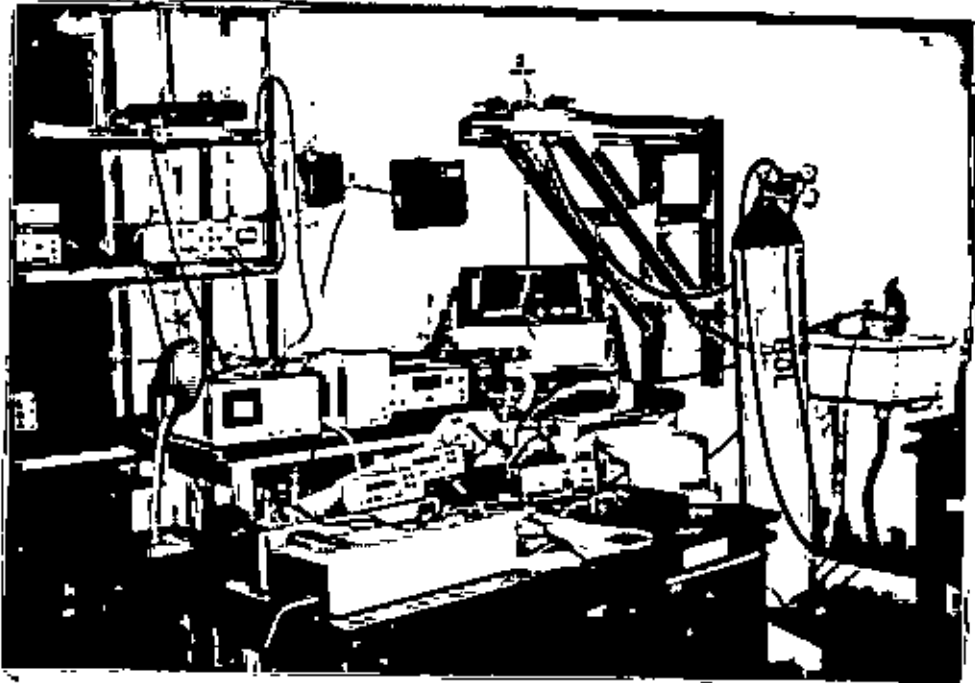
For cubic crystal the torque expressions with (110) and (111) planes are:

$$L_{(110)} = -\left(\frac{K_1}{4} + \frac{K_2}{64}\right) \sin 2\theta - \left(\frac{3K_1}{8} + \frac{K_2}{16}\right) \sin 4\theta + \frac{3K_2}{64} \sin 6\theta \quad (5.4)$$

and

$$L_{(111)} = \frac{K_2}{18} \sin 6\theta \quad (5.5)$$

Taking the measurements on a (100) crystal the constant K_1 may thus be obtained independently from the torque curve from the experimental amplitude of the sine wave.



Photograph of the Torque Magnetometer

5.2 Design and working principle of the Torque Magnetometer

The Torque Magnetometer which was initially studied and designed by Björn Westerstrandh, Uno Gafvert and Leif Lundgren of the Department of Solid State Physics of the University of Uppsala in Sweden in 1976 [40] was redesigned and constructed at Uppsala. The torque magnetometer of the Department of Physics at BUET was provided by the International Science Programs (ISP) through a research collaboration is used for the measurement of magnetic torque. A simple form of magnetic torque compensation is achieved by suspending the sample from a fibre with known torsional constant in to a magnetic field of known magnitude. When a magnetic field is applied on the sample, the sample aligns its direction of easy magnetisation with the magnetic field. When the sample is rotated away from the easy direction the sample resists this effort due to the magnetocrystalline anisotropy and thus exerts a torque. The torque from the crystal will twist the fibre on which the sample is suspended. The rotation of the sample is followed by the rotation of a mirror connected to the fibre. A laser beam is shined on the mirror which then illuminates a couple of photodiode. A small rotation of the mirror will give rise to an unbalanced photocurrent. This photocurrent is fed in to the (PID) regulator which is kept in the reverse biased mode generates a compensation current and sends to the compensating coil suspended in the permanent magnetic field of the torque head. Fig. 5.1 explains this phenomenon. Thus by measuring the compensation current through the coil we can measure the magnetocrystalline anisotropy of the sample. The torque from the sample is proportional to the compensating current through the coil. Thus we measure the current needed for the crystal to keep its orientation.

The principal drawing of the Torque magnetometer with an automatic compensation system is shown in Fig. 5.1. The sample is rigidly connected to a mirror and the compensation coil. The whole assembly is freely suspended in a thin quartz fibre and the coil is located in a field produced by a pair of permanent magnets. Now if a laser beam is shined on the mirror, the image of the beam will move as soon as some torque

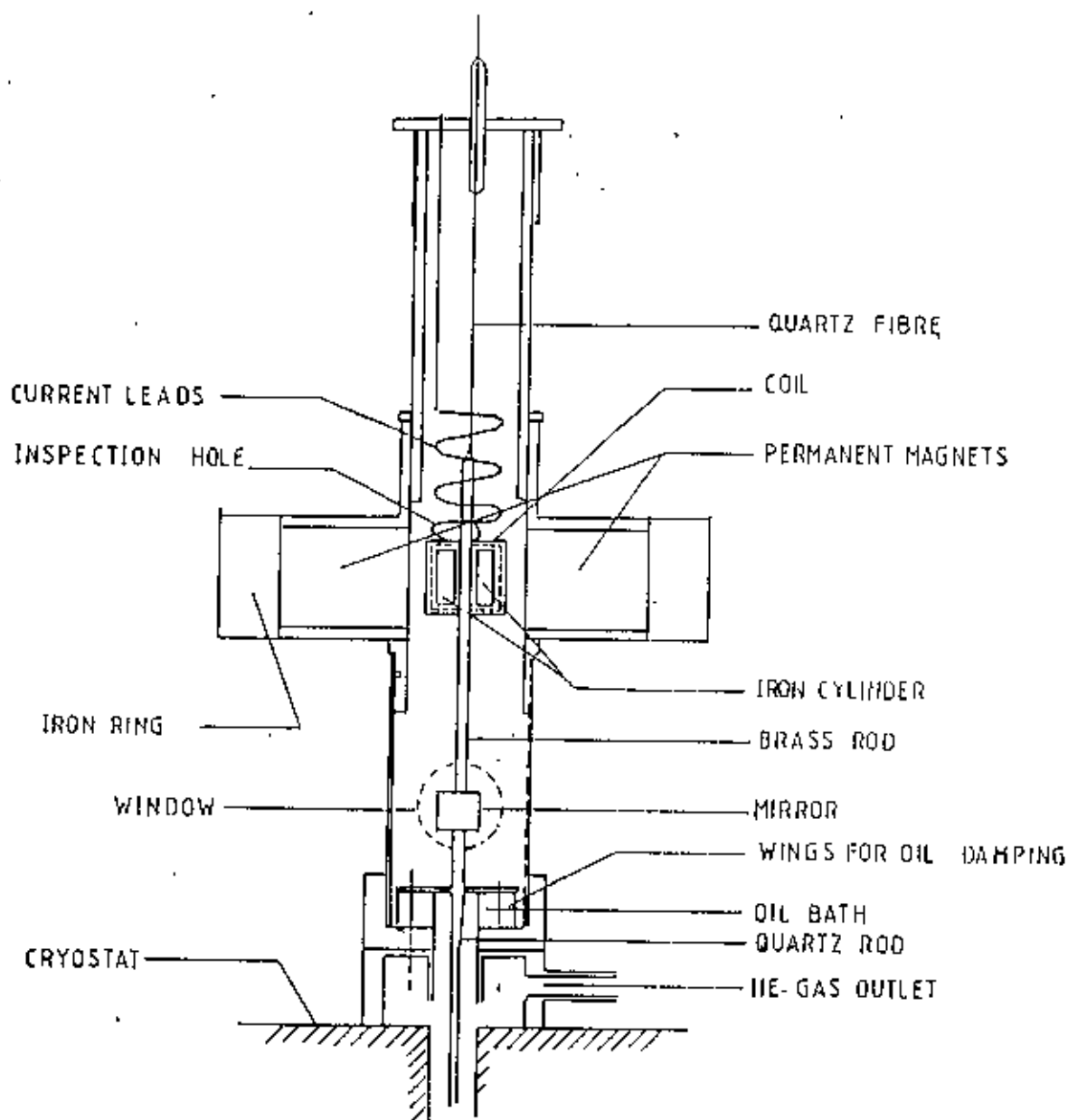


Fig. 5.1 Cross section of the upper part of the Torque Magnetometer

acts on the crystal and thus turns the mirror. The principle is to let a photo-detector detect the movement of the reflected beam via an amplifier generating a current through the compensation coil which inhibits the motion of the suspension.

The simplest type of electronic compensation system with a photo-sensitive feedback have been designed (Westerstrandh et al.). The simplest way is to let the current through the compensation coil be directly proportional to the signal from the detector. Such a feedback system is often referred to as a proportional (P) regulator. If a torque acts on the crystal the turning of the mirror gives rise to a deflection of the beam shining on the detector. The deflection from the centre of the detector can be made small by increasing the amplifier gain. Nevertheless the contribution from the rigidity of the suspension may seriously affect measurements of small torques. Neither the gain of the feedback could be increased too much since the system will then become unstable. To improve the stability we have used the oil damping. The viscosity of the oil damps oscillations so that we can increase the amplifier gain. To enhance the electronic damping a differentiating amplifier has been used in parallel with the proportional amplifier and hence improve the stability of the system. This type of compensation system can be characterised as a proportional differentiating regulator (PD). Since the large deflection of the suspended system is a problem, the introduction of a differentiating unit allows a very high gain and a small angular deflection.

5.3 Measurement of magnetic anisotropy by Torque Magnetometer

For measurement of magnetic anisotropy by torque magnetometer, at first the sample the form of a circular disc is prepared. The circular disc is then fixed on a sample holder for magnetic torque measurement. The sample holder is hung on a quartz fibre

fixed with the upper part of the torque magnetometer. A small magnetic field is applied on the sample to measure the response of the sample. The signal from the sample is recorded through an electronic compensating system. The noise from the electronic system is eliminated by regulating the proportional gain (P), integrating time constant (I), and the differentiating time constant (D). Once the signal is stabilized, the magnetic field is increased in steps of one kilo gauss up to maximum of 4 kilo gauss. The magnetic field is rotated in steps of 10° for a complete 360° rotation. For every 10° rotation of the magnetic field, the magnetic torque is recorded. Thus the torque data is recorded for 36 angular positions of the magnetic field. These 36 points are entered in a computer for Fourier analysis. The Fourier coefficients A_0 , A_2 and A_4 are calculated. The Fourier coefficients are plotted against the reciprocal of the applied magnetic field (i.e., $\frac{1}{H}$). The extrapolated values of the coefficients for $\frac{1}{H} = 0$ are taken as the values at the saturation field. The signals are found to obey a $\sin 4\theta$ curve. Thus only A_4 coefficients are found dominating.

5.4 Sample preparation

Pure Ni single crystal was procured from the National Bureau of Standard (N.B.S). The crystal is cut in the (100) crystallographic plane. Thus the plane contained only [100] and the [110] crystallographic directions. The (100) crystallographic plane is confirmed by orienting the sample using the Laue photographic technique. Since evaluation of K_1 is the purpose of this work, the sample plane is chosen to be (100) crystallographic plane to avoid any contribution from the second anisotropy constant K_2 . The sample is found to have the mass $m = 45.6 \times 10^{-6}$ kg and volume $v = 5.11 \times 10^{-9}$ m³.

5.5 The sample suspension

The sample is mounted at the end of a thin quartz rod. Quartz is a suitable material for this purpose as it is diamagnetic and has a low thermal conductivity. The upper end of the quartz rod is attached to a brass rod to which the mirror and the compensating coils are fixed. The whole assembly is suspended in a quartz fibre. The quartz fibre is very suitable for this purpose because of its large tensile strength and small torsional constant. Typical value of the torsional constant is $5-20 \times 10^{-7} \text{ Nm/rad}$. The elasticity in the longitudinal direction is very low, which prevents low frequency oscillation along the axis of suspension. The compensation coils have 10 layers of 100 turns of 0.06 mm copper wire. To minimise influence from the stiffness of the copper wire, the leads to the coils have been spiralled. Below the coil there is besides the mirror, an arrangement for oil damping, which damps the self oscillations.

5.6 Calibration of the Torque Magnetometer

For the calibration of the Torque magnetometer a thin nickel single crystal disc is used. The disc is of mass 45 mg. and is oriented in such a way that the (100) crystallographic plane lies on the plane of the disc. The sample is glued to a sample holder and is suspended from a thin quartz fibre connected to a brass spindle. The sample is then placed in between the poles of an electromagnet. A 3.0 kilo gauss magnetic field which is strong enough to saturate the nickel specimen is applied along the plane of the disc and measurements of torque is taken at every 10° angular rotation for a complete 360° rotation of the magnetic field. A total of 36 data points are obtained for a complete rotation of the magnetic field. The whole process of measurements is repeated for an

applied magnetic field of 3.5 kilo gauss and 4.0 kilo gauss. The measured data are entered in a computer for Fourier analysis. The Fourier coefficients are then equated with the standard equation for torque curve. Thus from the known mass of the disc and the known value of the anisotropy constant for nickel at room temperature, the calibration constant of the torque magnetometer is determined.

5.7 The High Temperature Oven

The most important feature in the construction of the oven is that the inner stainless steel tube extends throughout the oven and the thermocouple unit is introduced from the bottom end with the thermocouple junction placed immediately below the sample. The heater is wound directly on the inner tube. The heater consists of a MgO insulated Chromel-Constantan thermocouple with a stainless steel cover (O.D. 1 mm, length 1.3 m, manufactured by OMEGA Corp. This thermocouple is flexible, and to obtain a firm contact between the heater and the inner sample tube, the thermocouple is first wound on a tube with a somewhat smaller diameter and the resulting spiral is afterwards squeezed on to the sample tube. The thermal contact between the heater and the sample tube is improved by adding some silver paint. The lower ends of the heater wires are electrically connected by means of silver paint. Copper wires, connecting an external power supply, are soft soldered on the upper ends of the heater wires. The silver paint is dried out at ordinary atmosphere by passing some current through the heater. The advantages to use this Chromel-Constantan thermocouple as a heater for this oven are that it is readily available, non-magnetic, insulated, easily formed and gives a bifilar winding and close thermal contact with the sample tube. The heater has a resistance of 75 Ω at room temperature.

Five radiation shields, consisting of 50 μm stainless steel foils are located outside the heater. These are tied directly on to the heater using reinforced glass fibre threads. The outer tube is at the bottom end connected to the inner tube via a phosphor-bronze bellow in order to allow for the difference in length of the two tubes at higher temperatures. O-ring couplings are used throughout to enable easy disassembling of the oven in case of any fault.

Both the oven and the thermocouple are adjustable in height with respect to the sample. This gives a possibility to find a position of the sample in the warmest region of the oven which gives a minimum temperature gradient between the sample and the thermocouple junction. The temperature gradient $\frac{\Delta T}{T - T_0}$ over 10 mm of length in the warmest part of the oven is approximately 0.1% and independent of the temperature.

The special characteristics of the oven are:

- (i) the oven can be heated from room temperature to 1043 K in less than 15 minutes with a temperature difference between thermocouple and sample of less than 1 K at the final temperature.
- (ii) at a constant heating or cooling rate of 5 K/minute a temperature difference of the order of 1 K is established.
- (iii) Due to small thermal mass of the oven, it cools from 1150 K to 600 K in about 30 minutes which enables a fast interchange of samples.

92923

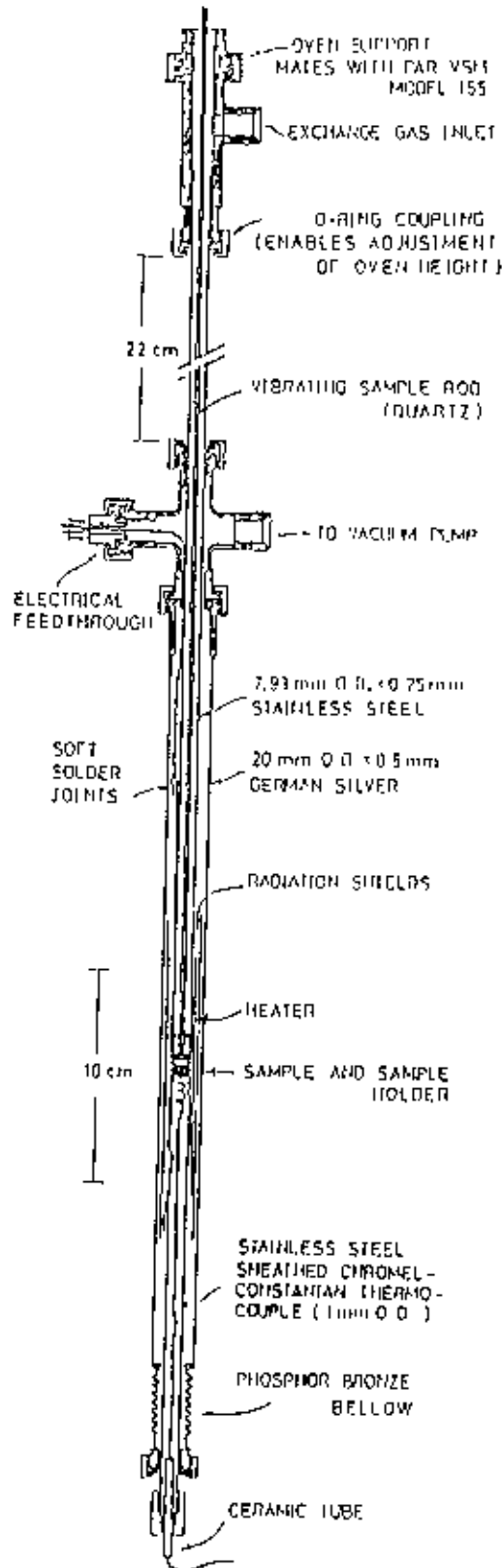


Fig. 5.2 Schematic diagram of the high temperature oven

5.8 Evaluation of the torque curve by Fourier analysis

The measured values of the magnetic torque are fed in to an IBM 486 personal Computer for Fourier analysis. The Fourier coefficients are evaluated using a programme written in MS Basic language designed specially for the analysis of magnetic torque data. The input data are the torque in volt (τ), and the corresponding angle (θ). The analysis also gives the offset angle of the magnetic field, which may be adjusted by rotating the magnet through the offset angle to locate the zero torque position. The evaluated Fourier coefficients are the values at the saturation field, and are used to calculate the anisotropy energy of the sample. This anisotropy energy is the energy difference between the easy direction of magnetisation of the sample and the hard direction of magnetization. Using the mass of the sample and the calibration constant of the torque magnetometer, the anisotropy constants is evaluated.

5.9 Magnetization process of Nickel

Magnetization is defined as the magnetic moment per unit volume. There are various ways of measuring magnetization of a substance. In present thesis magnetization is measured at room temperature by using a Vibrating Sample Magnetometer (VSM)[41].

The measurement of magnetization is usually performed by measuring magnetic moment of a specimen and deviding this quantity by the volume or mass of the specimen. The techniques for the measurement of magnetic moment by the direct methods can conveniently be classified into two categories:

- (1) The measurement force exerted on the magnetic moment of the specimen by an inhomogeneous field and
- (2) The measurement of the emf induced by the suitable coil system by changing relative position of the magnetic moment with respect to the coil system or by varying the magnetic moment.

The VSM is a highly sensitive and versatile equipment for measuring the magnetic moment, magnetization and magnetic susceptibility. The VSM was invented by Van Osterhout [42] and simultaneously and independently by S. Foner [43-44]. The basic principle of VSM developed by Foner is based on the flux change in a coil when the sample is vibrated near it. The sample, usually a small disc is cemented to the end of a rod, the other end of which is fixed to a loud speaker cone (as shown in Fig. 5.3) or to some other kind of mechanical vibrator.

Current through the loud speaker vibrates the rod and the sample at about 80 cycle/sec and with an amplitude of about 0.1 mm in a direction at right angle to the magnetic field. The oscillating magnetic field of the sample induces an alternating emf in the detection coils. The vibrating rod also carries a reference specimen in the form of a small permanent magnet near its upper end induces another emf in two reference coils. The voltages from the two sets of coil are compared and the difference is proportional to the magnetic moment of the sample. The VSM used in the present work to take the magnetization measurement is of Foner type. The Magnetic Materials Division, Atomic Energy Center, Dhaka designed and constructed this Foner type VSM in 1986.

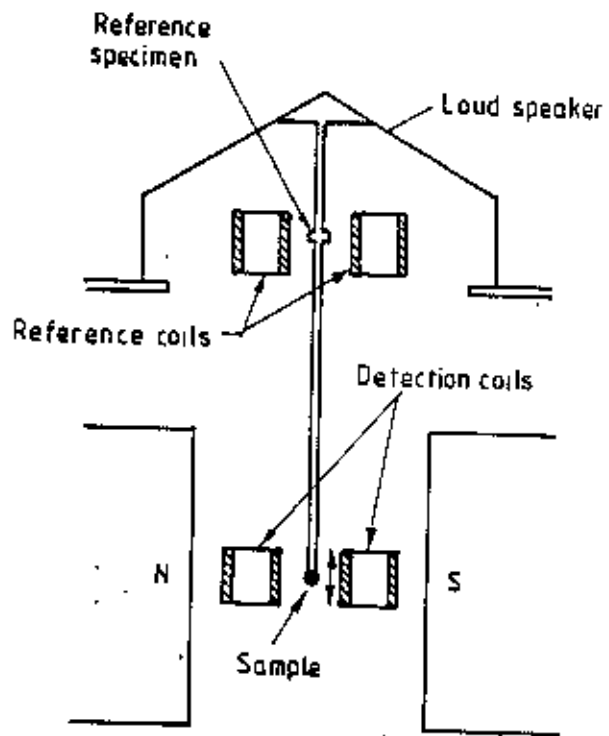


Fig. 5.3 Vibrating Sample Magnetometer (Foner type)

5.10 The working principle of the Vibrating Sample Magnetometer (VSM)

A schematic diagram of the VSM including the various mechanical and electronic parts is shown in Fig. 5.4 to illustrate the basic working principle of the unit. The signal generator SG feeds a sinewave signal of 80 Hz frequency to the audio amplifier AA which in turn drives the speaker SP. The output of the signal generator is also connected to reference channel input of the lock-in-amplifier LA. The drive-rod assembly R tightly coupled to the vibrating papercone of the speaker vibrates in a vertical direction along its length. The amplitude of vibration may be varied by changing the gain of the audio amplifier. A permanent magnet P of cylindrical shape is fitted to the drive-rod at its lower end with the help of a sample holder H. Two cylindrical sample coils SC with their axes kept vertically are placed on the opposite sides of the sample and along the line joining the centres of the poletips (N.S.) of the electromagnet. They are connected in series opposition and the net output signal is connected to the lock-in-amplifier through a shielded cable. This pair of coils is referred to as the sample coil system. Another pair of coaxial coils RC also connected to each other in series opposition is placed symmetrically around the permanent magnet P. This coil pair is the reference coil system.

As the drive-rod assembly is vibrated with a particular frequency and amplitude, the sample S induces a signal of the same frequency in the sample coil system. This signal is proportional to the dipole moment of the sample. As the field in the pole-gap is gradually increased by increasing the current through the electromagnet, the sample becomes magnetized more and more and induces a larger signal in the sample coil system till it reaches saturation magnetization.

This signal directly goes to one of the inputs of the lock-in-amplifier. Similarly, another signal of the same frequency is induced in the reference coil system due to vibration of the permanent magnet P. Since moment of the magnet is fixed, the signal is also of fixed amplitude for a particular frequency and vibration amplitude. This signal is the

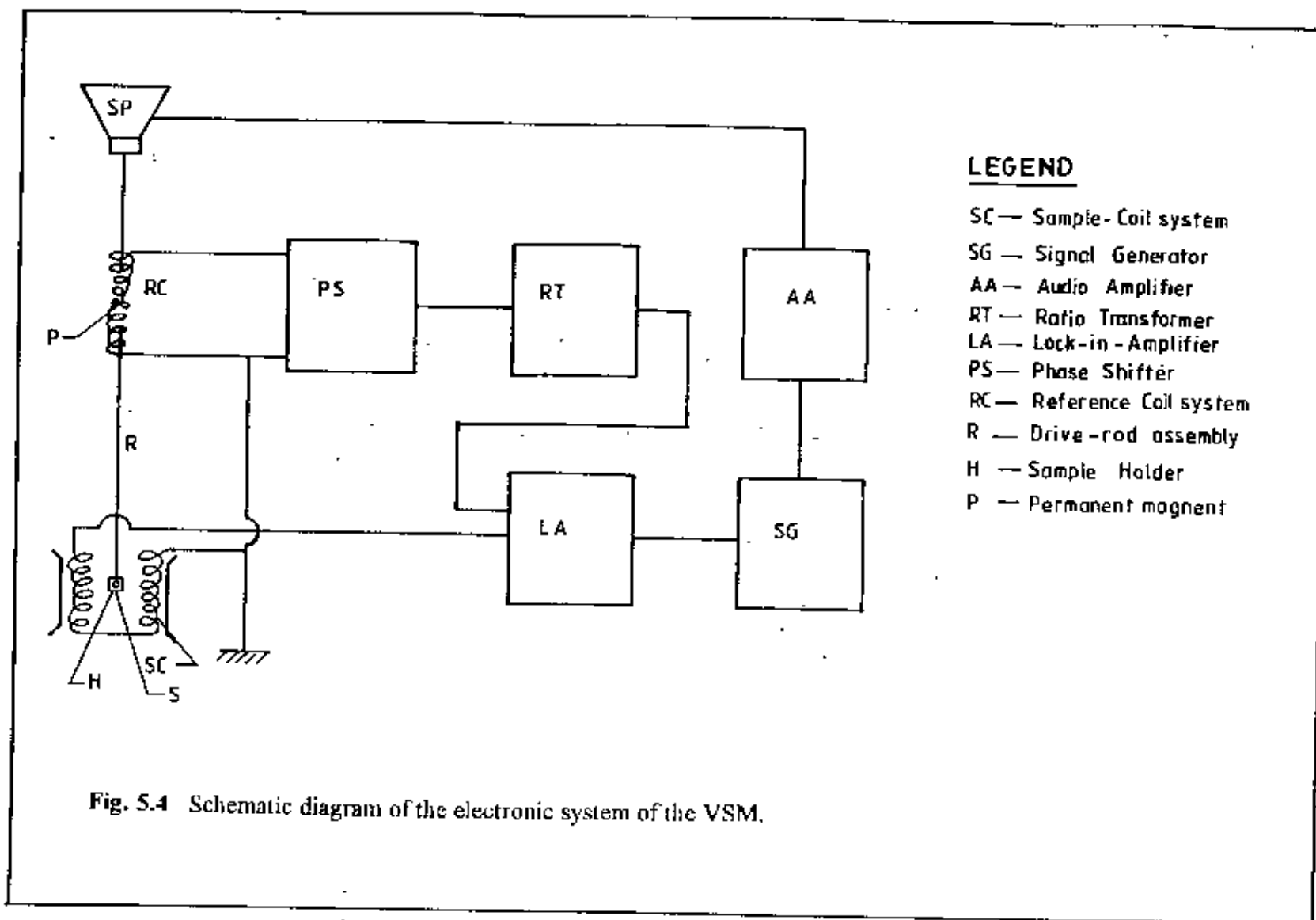


Fig. 5.4 Schematic diagram of the electronic system of the VSM.

reference signal and it is first fed to a unity gain phase-shifter unit. The phase-shifter capable of continuously changing the phase from 0° to 360° , is used to bring the reference signal in phase with the sample signal.

From the phase-shifter the reference signal passes on to the decade ratio transformer RT, of constant input impedance. The output of this transformer then goes to the other input of the lock-in-amplifier. The output to input ratio of the decade transformer can be accurately varied from 10^{-8} to 1. By turning various knobs of the decade transformer the amplitude of its output is made equal to that of the sample signal. The lock-in-amplifier is operated in the differential input mode and is used as a null detector. When the sample signal and output signal of the decade transformer are of equal amplitude and in the same phase, the d.c. meter of the lock-in-amplifier gives a null-reading. The whole electronic system then correctly measures the ratio of the sample signal to the reference signal. Since sample S and the permanent magnet P are vibrated with the same drive-rod assembly, the sample-signal and reference-signal have direct phase and amplitude relationship. As a result the ratio of the sample signal to the reference signal is proportional to the magnetic moment of the sample. The measurement is insensitive to small changes in the amplitude and frequency of vibration and the gain of the amplifier. The accuracy of the equipment depends mainly on the accuracy of the ratio transformer and the gain of the amplifier.

5.11 Description of mechanical design of the VSM

The various mechanical parts of the magnetometer are described in detail in the Fig.5.5. The base B of the VSM is a circular brass plate of 8 mm thickness and 250 mm diameter. A brass tube T of 25 mm outer diameter and 0.5 mm thickness runs normally through the base such that the axis of the tube and the centre of plate

coincide. The base tube are joined together by soft solder. The tube extends 60 *mm* upward and 24 *mm* downward from the base. There is a vacuum port on the lower part of the tube 120 *mm* below the base. The lower end of the tube T is joined to a brass extension tube I. by a threaded coupling and an O'ring seal. Another thin tube K made of german silver and of 8 *mm* inner diameter runs through the extension tube I. from the coupling point C to about 50 *mm* below the sample position. Above the base there is a hollow brass cylinder M of 180 *mm* length and 130 *mm* inner diameter and having 40 *mm* wide collars at its both ends. The lower collar seats on an O'ring seal which is situated in a circular groove in the base plate. On the upper collar, there rests an aluminium top N with an O'ring seal. The brass cylinder M has a side port VP. This is again a brass tube of 41 *mm* diameter and 43 *mm* length. The port has a collar at the end away from the cylinder. A perspex vacuum feed-through is fitted at its end with O'ring seal. This port is connected to the cylinder by soft solder.

Electrical connections from the audio amplifier to the speaker and from the reference coil system to the phase-shifter are taken via the perspex feed-through. By connecting the vacuum port of the tube T to a vacuum pump the sample environment can be changed. The speaker SP is fitted 25 *mm* above the tube T with the help of our brass stands. The lower ends of stands are screwed to the base plate while the rim of the speaker is screwed on the top of the stands. The speaker has a circular hole of 10 *mm* diameter along the axis of it. An aluminium disc having female threads in it is fitted to the papercone with araldite. The aluminium connector having male threads on it and attached to the drive rod assembly fits in the aluminium disc and thus the drive rod assembly is coupled to the speaker. The drive rod assembly consists of detachable parts which joined together by means of aluminium threaded connectors. Each part is a thin Pyrex glass tubing of 4 *mm* diameter. The upper part has a small permanent magnet P situated 100 *mm* below the aluminium connector attached to it. At the lower end of the drive rod assembly a perspex sample holder having quite thin wall can be fitted tightly with sample in it. A few perspex spacers are also attached to the driver-rod throughout its length. The spacers guide the vibration of the sample only in the vertical

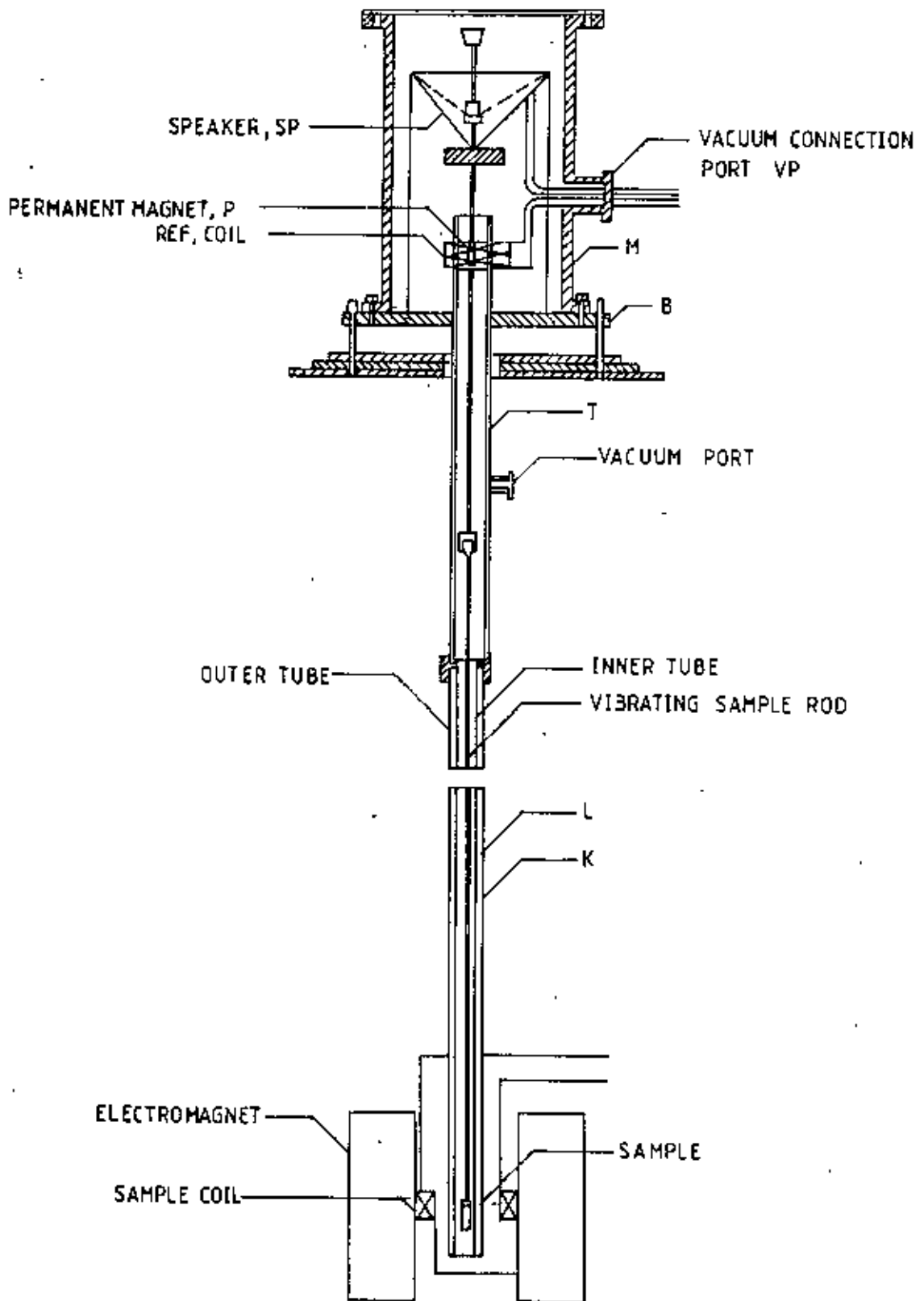


Fig. 5.5 Mechanical design of the VSM.

direction and stops sidewise vibration or motion. The total length of the drive-rod assembly is 920 mm.

The base plate of the VSM rests on three levelling screws above a brass frame which in turn rests on an iron angle bridge. The bridge rigidly fitted to the sidewall of the room. The brass frame is provided with arrangements with the help of which it can be moved in two perpendicular directions in the horizontal plane. The levelling screws are used to make the drive-rod vertical and to put the sample at the centre of the pole-gap between the sample coils. The sample can also be moved up and down by the levelling screws.

5.12 Calibration of the VSM

There are usually two methods of calibration of a VSM.

- (1) by using a standard sample and
- (2) by using a coil of small size whose moment can be calculated for d.c. current through it.

The magnetometer is calibrated using a standard spherical sample of nickel having 99.9% purity. The sample was made spherical with the help of a sample shaping device. It was then annealed in helium atmosphere at about 900°C . The sample's saturation magnetic moment has been calculated using the available data. The ratio-transformer reading is obtained by *in situ* measurements and thus the value of the calibration constant K is obtained.

The accuracy of this calibration, however, depends on the reliability of the standard nickel sample, the accuracy of the ratio transformer and the gain of the amplifier. The

equipment has been operated repeatedly with the same standard sample and finally stability has been found to be within 1 in 1000.

The sensitivity of a VSM is usually determined by the signal to noise ratio. But because of comparatively low sensitivity of the lock-in-amplifier used in this equipment, the noise level could not be measured. The maximum sensitivity of the lock-in-amplifier is 10 microvolt (r.m.s). So the differential method has been used to measure the sensitivity. It is found to be about 10^{-4} emu. It may be mentioned here that the sensitivity of a commercial VSM made by PARC (Princeton Applied Research Corporation, USA) is 5×10^{-5} emu.

With the sensitivity so far achieved, this VSM can be used for investigation of only ferromagnetic and strongly paramagnetic materials at room temperature. In order to extend its usefulness, a more sensitive lock-in-amplifier, a sample oven and a cryostat are needed.

5.13 Measurement of magnetization of Nickel by VSM

The basic principle of a VSM is to measure the magnetization and compare this measured signal with a standard reference sample. When a magnetic sample is vibrated in a magnetic field an induced electromotive force (e.m.f) is generated in a coil placed near to the vibrating sample based on the principle that a change in the magnetic flux gives rise to an induced e.m.f. and vice versa. This induced e.m.f is fed in to a Lock-in-Amplifier. Another e.m.f. of known magnitude is generated by another sample of known mass and known magnetic moment which is vibrated by common member. The two signals are compared by a Lock-in-Amplifier and their phase and sensitivity are

adjusted. Once the signals are in phase, the Lock-in-Amplifier gives a zero output. The measured signal is the signal from the sample under investigation.

The measurement of magnetization of Ni single crystal was performed using a vibrating sample magnetometer as shown in Fig. 5.5. Sample in the form of thin disc of diameter 5 mm was prepared from the disc shaped sample. The specimen was glued to the sample holder of the VSM. Measurements of magnetization was taken at room temperature for different values of the magnetic field in the range 0.1 *kilo gauss* to 4.0 *kilo gauss*. The magnetic field was simultaneously measured with the help of a Digital Gauss-Meter.

5.14 Evaluation of magnetic moment data of Nickel

Before gluing the Ni specimen under investigation with the sample holder, the calibration constant of the VSM was measured using a 99.99% pure nickel polycrystalline specimen. The calibration constant was found 7.45 emu. Then this sample was removed and the single crystal of Ni was mounted. Initially with the increase of the magnetic field the magnetization increased. At one stage the magnetization attained a constant value. This value is considered as the saturation magnetization.

Chapter 6

Results and Discussion

As a soft magnetic material Nickel could easily be saturated by applying a magnetic field of 4 kilo gauss strength. Thus all of our measurements are assumed to have been done at saturated field. The Ni disc is oriented in the (100) crystallographic plane and thus we obtained the $\sin 4\theta$ curves in all the torque measurements. After performing Fourier analysis of these curves the K_1 values are calculated. The measured torque curves are found to be field independent above the saturation field. The order of harmonics higher than 4θ are ignored as these had very little or no affect on the calculation of the first anisotropy constants. Harmonic analysis of the experimental torque curves taking different positions as the origin may yield the coefficients of the higher order harmonics. Plotting the coefficients of the higher order harmonics against the positions of the origin one can have a curve which may give an information about the beginning of the higher order coefficients. It is also possible to minimise errors that are inherent in computing the harmonic coefficients with a finite number of terms taking different combination of points on the curve in each time.

Fig. 1 shows the magnetic torque curves of Nickel at different applied magnetic fields at the room temperature (298 K). The sample is gradually brought to saturation by applying the magnetic fields of increasing magnitude. The saturation field is estimated to be around 4 kilo gauss. This is done by plotting the values of K_1 against $\frac{1}{H}$ and extrapolating the curve to $\frac{1}{H} = 0$. The values of K_1 at this point is taken to be the values at the saturation field. The sign of K_1 is found to be negative. The sign of K_1 and its decrease in magnitude with temperature indicates a greater temperature dependence of K_1 . Fig. 2 shows the magnetic torque curve at the saturation field. A

total of 36 data points are taken at an interval of 10 degrees for a complete 360° angular rotation of the (100) crystallographic plane. Since there are few higher order harmonics in a Ni torque curve, it is possible to obtain an accurate value of K_1 by calculating upto $\sin 4\theta$ terms. Fig. 3 shows the magnetic torque curves of Nickel at different temperatures at the saturation field. Although there is no change in the periodicity of the torque curves, the torque magnitude is found to decrease with temperature. This indicates that the sample is approaching the ferromagnetic Curie temperature (T_c), where the magnetic anisotropy is practically zero and the sample enters in to the paramagnetic phase. This fact agrees qualitatively with the Zener's theory of magnetic anisotropy. Fig. 4 shows the torque curves of Nickel around and above the Curie temperature. The upper curve shows that there is a possibility of rotation of the crystal easy axis as the thermal agitation takes over the magnetic anisotropy of the system at this temperature. Fig. 1, 2, and 3 show the $\sin 4\theta$ torque curves which are responses mainly for the (100) crystallographic plane, while the lower curve of Fig. 4 shows a combination of $\sin 2\theta$ and $\sin 4\theta$ curves which is a response for the (110) crystallographic plane. Therefore we predict that a rotation of the easy axis has occurred near the Curie temperature. Fig. 5 shows the temperature dependence of the first anisotropy constant K_1 of Nickel. The values of K_1 decreased quite sharply at the lower temperature region but takes a monotonic fashion at higher temperature region as the sample approaches the Curie temperature. The temperature dependence of magnetocrystalline anisotropy arises because of the deviation of the local spin axis from the average magnetization direction. This happens because with increasing temperature the spin axis deviate from the direction at absolute zero due to thermal agitation. The whole effect is reflected in the lagender polinomial of the 4th order. Comparing the results of R. R. Birss [13] on magnetization of Ni as a function of temperature with our results of anisotropy constants as a function of temperature we can say that the anisotropy constant falls off quite faster than the magnetization. Our results although shows temperature dependence of anisotropy constants do not quite agree to the theoretical predictions which did not take into account thermal expansion

of the crystal. Table 1 shows the values of anisotropy constant K_1 in different temperatures. The magnetic anisotropy practically goes to zero at the ferromagnetic Curie temperature. According to Zener the first anisotropy constant and the saturation magnetization is related as $\frac{K_1(T)}{K_1(0)} = \left[\frac{M_s(T)}{M_s(0)} \right]^{10}$ however, this relation is experimentally found to hold good for iron which has the [100] crystallographic direction as the direction of easy magnetization. For Nickel which has the [111] crystallographic direction as the direction of easy magnetization, the above relation is not found to hold good. The fall of anisotropy with increasing temperature is faster for nickel than for iron. The temperature dependence of magnetostriction is also faster for Ni than for iron and cobalt. Fig. 6 shows the M vs H curve for Nickel at room temperature. The magnetization curve at lower magnetic field is quite sharp which is an indicative of the high quality of the sample. At $H = 1945$ gauss it becomes saturated and there is no rise of magnetization even if the magnetic field is raised further. Table 2 shows the values of magnetization at room temperature. It is observed that the variation of anisotropy is quite faster near the low temperature region than that nearer to the Curie temperature.

Table 1: Values of anisotropy constant K_1 in different temperatures

Temperature (in K)	Anisotropy constant K_1 (in J/m^3)
298	-4.52×10^3
326	-3.18×10^3
351	-2.23×10^3
374	-1.63×10^3
404	-0.92×10^3
433	-0.56×10^3
446	-0.42×10^3
454	-0.39×10^3
463	-0.35×10^3
478	-0.24×10^3
498	-0.16×10^3

Table 2: Magnetization Values for Ni single crystal at room temperature

Field Intensity (in Gauss)	Decatran Reading	Magnetic Moment (in <i>emu / gm</i>)
198	.1836	29.99
319	.2440	39.86
512	.2950	48.19
994	.3300	53.91
1487	.3348	54.69
1945	.3359	54.87
2430	.3360	54.89
3043	.3360	54.89

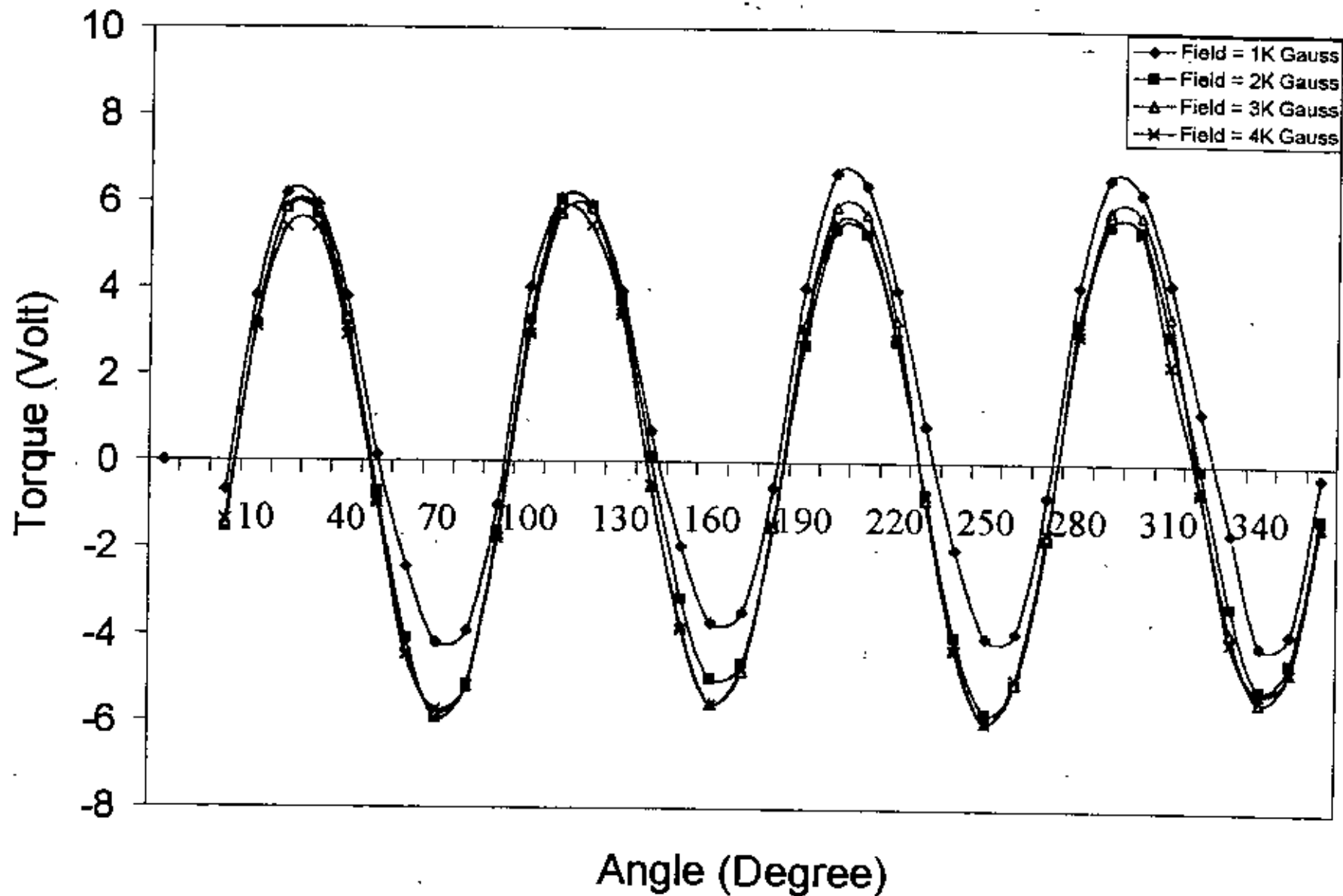


Fig. 1 Magnetic torque curves of Nickel at room temperature (298K)
Applied magnetic field $H=1, 2, 3, 4$ kilo gauss

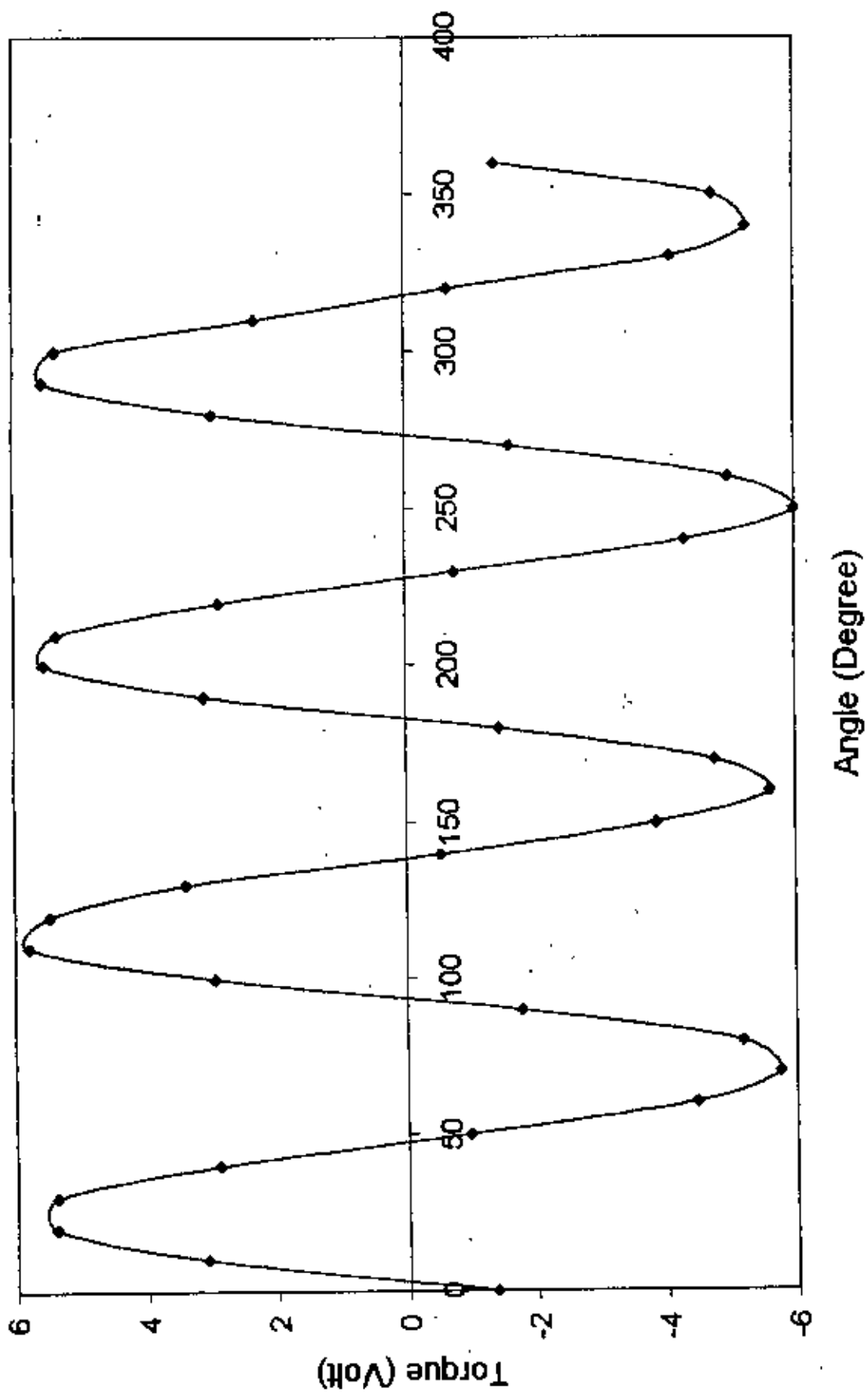


Fig. 2 Magnetic torque curve of Nickel at room temperature (298K) in the saturation field

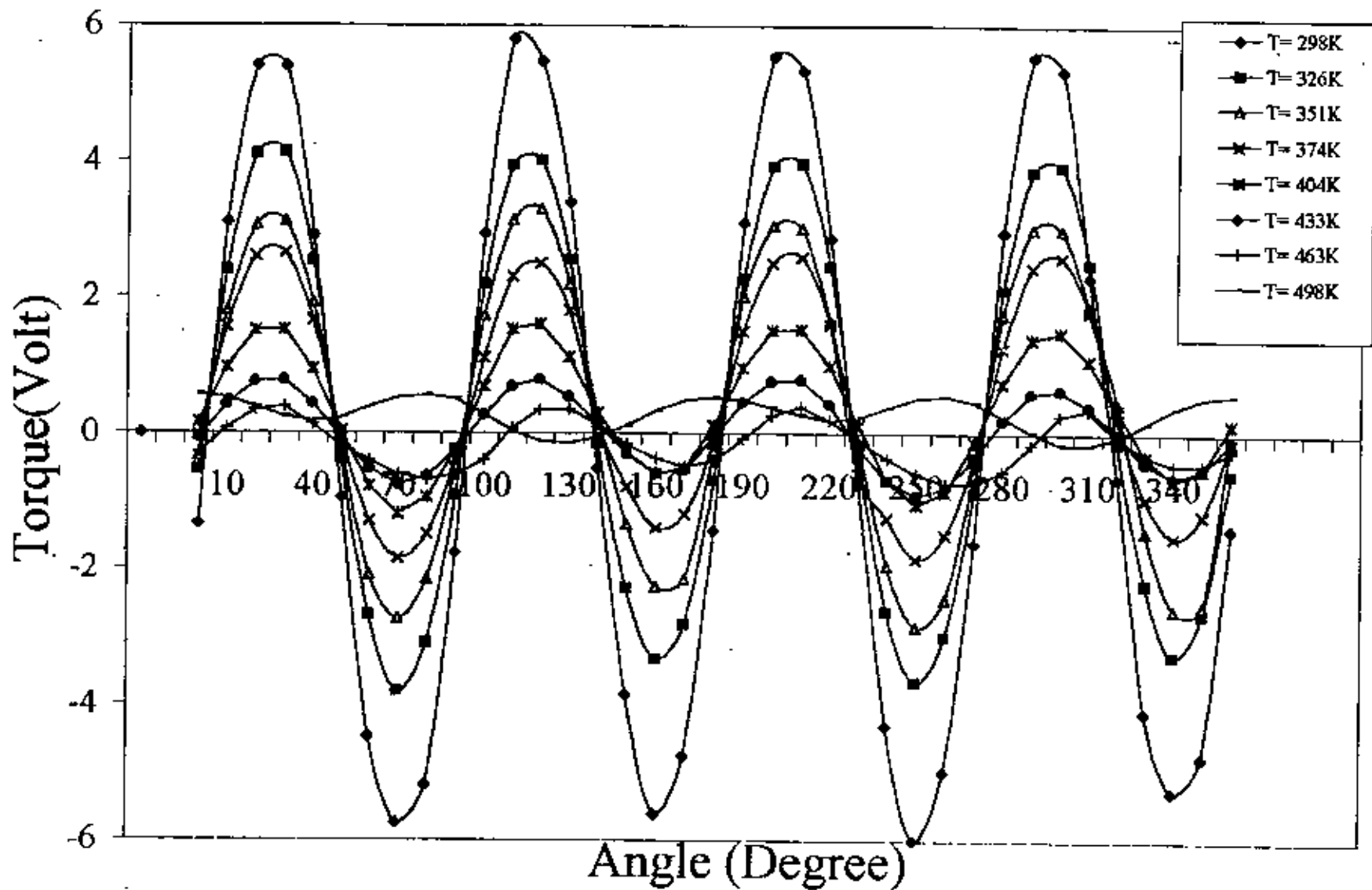


Fig. 3 Magnetic torque curves of Nickel at different temperatures
Applied magnetic field $H=4$ kilo gauss

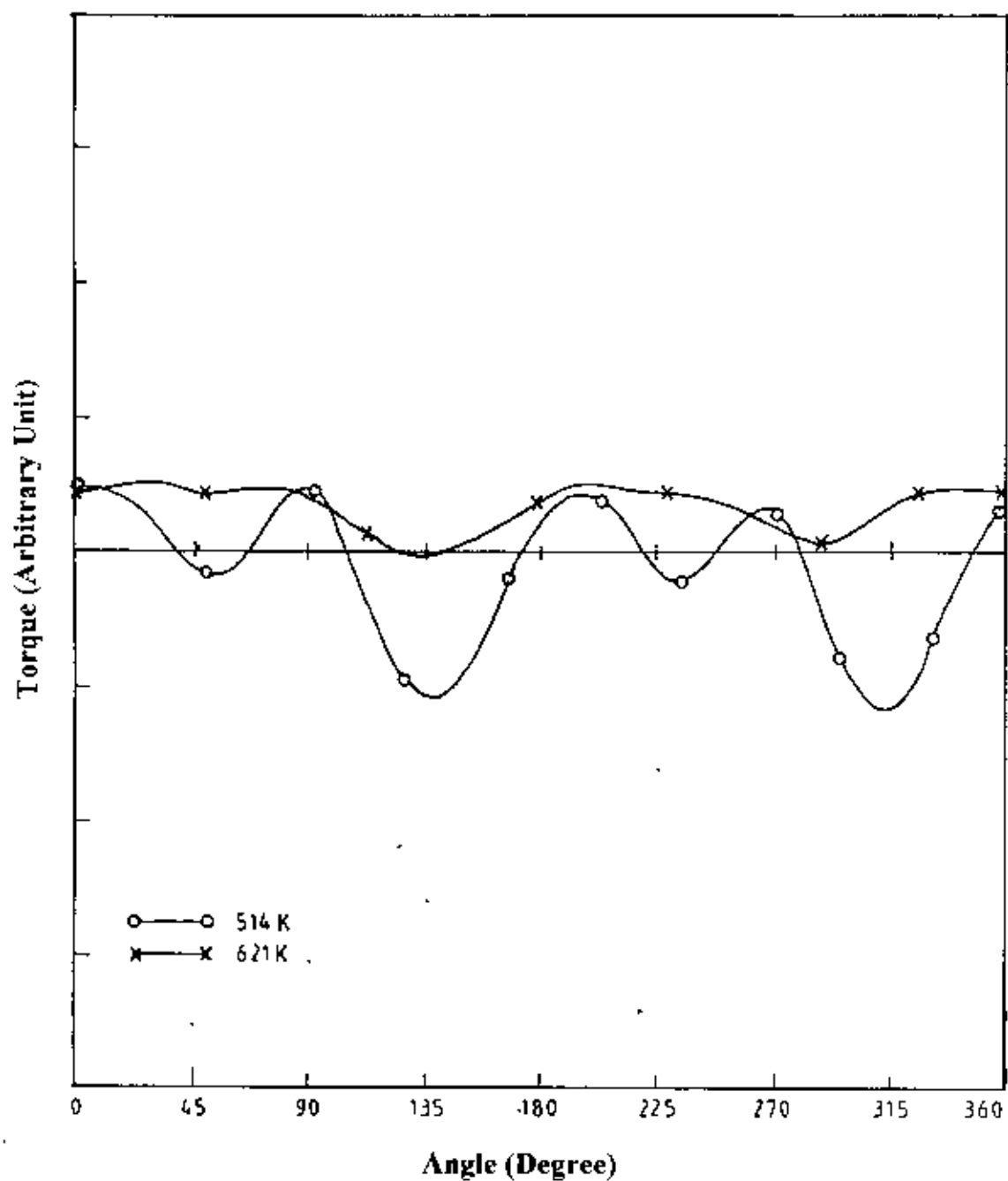


Fig. 4 Magnetic torque curves of Nickel around Curie temperature (627K)
Applied magnetic field H=4 kilo gauss

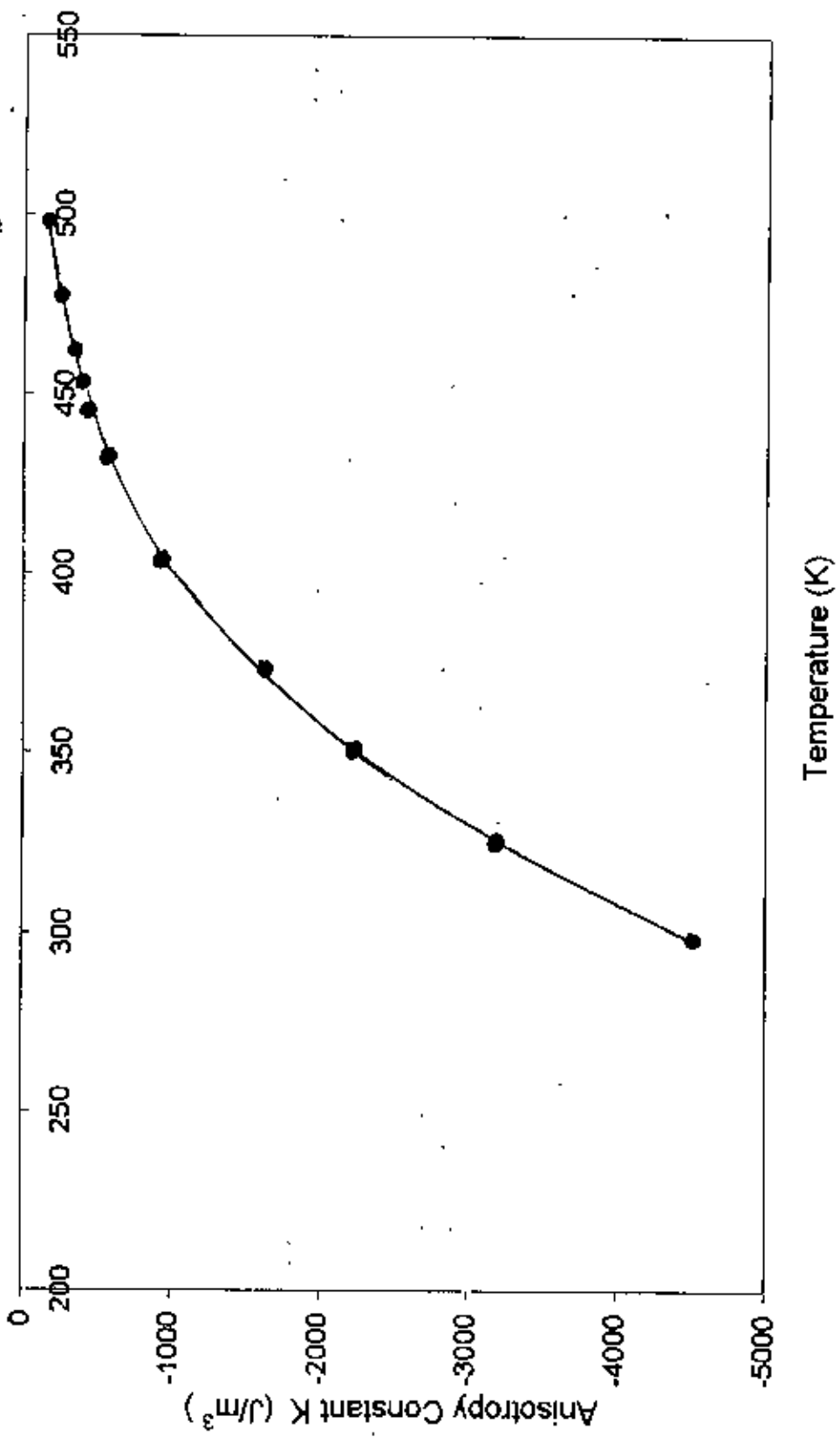


Fig. 5 Temperature dependence of K_1 for Nickel
 Applied magnetic field $H = 4$ Kilo gauss

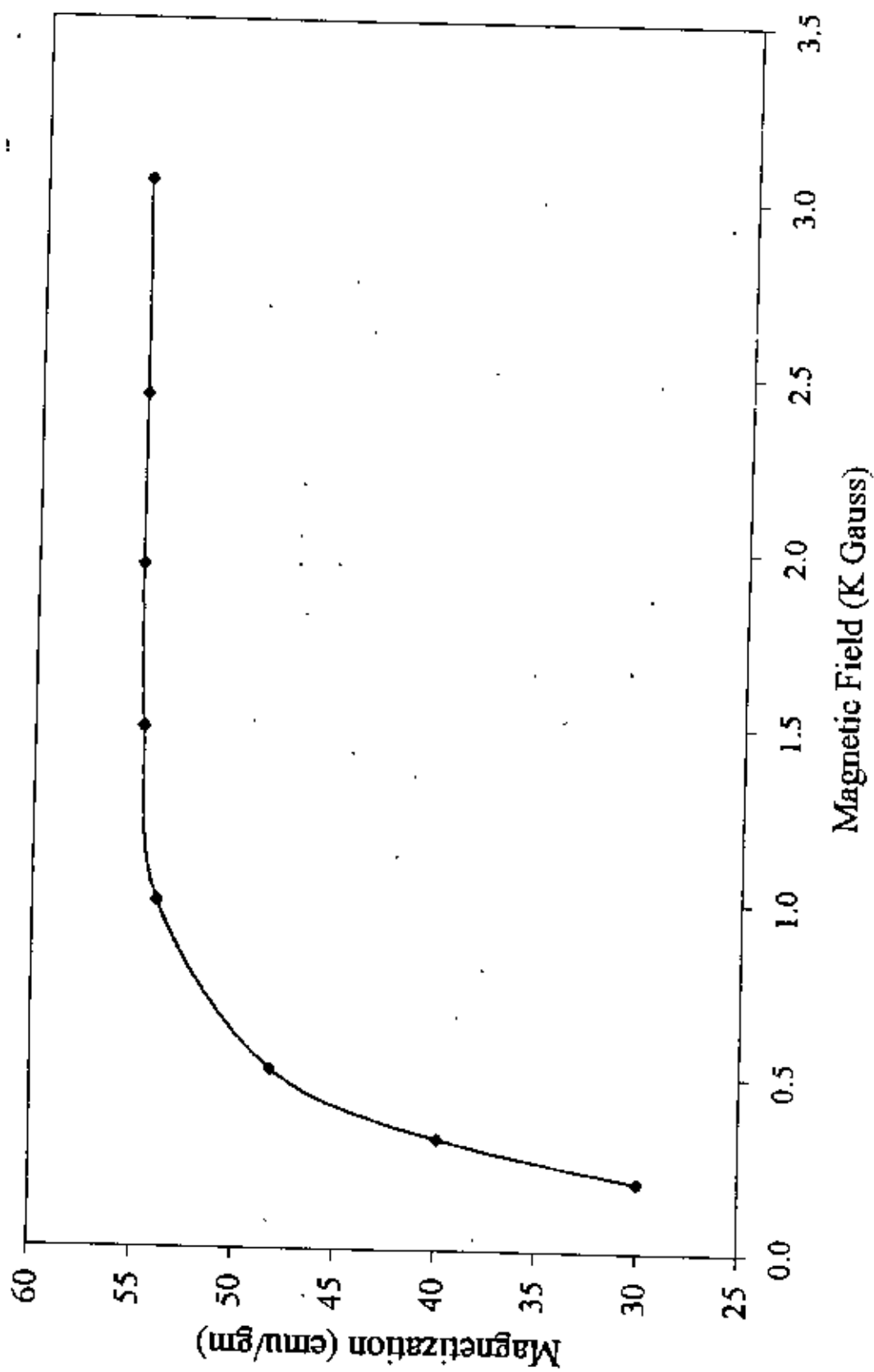


Fig. 6 Magnetization versus Magnetic field curve of Nickel

Conclusion

The anisotropy constants of Nickel decrease very rapidly with increasing temperature at low temperature. This nature is changed at higher temperature; however the rate of fall of anisotropy energy is slower in nature than it is at low temperature region. This work is an attempt to understand this marked temperature dependence of the magnetic anisotropy of Ni at high temperature. The interpretation of the high temperature property of magnetic anisotropy is given on the basis of experimental results.

The errors in orientation giving rise to $\sin^2\theta$, $\sin^4\theta$, $\cos^2\theta$ and $\cos^4\theta$ are ignored as these did not affect the values of the anisotropy coefficients. However, the torque arising from the asymmetric mounting of the specimen are not negligible as they may disturb the torque relations at higher temperature. For nickel it is observed that the change in the anisotropy constant is much too large in comparison with the magnetization. For the determination of the coefficients accurately it is found to be important to be careful about three factors, namely, the importance of the higher order terms of the coefficients, the importance of the purity of the specimen under investigation and the effect of strong temperature dependence. Also it is very important to know the fine details of the energy band structure in order to express the significance of the higher order coefficients. For nickel the first anisotropy constant K_1 decreases much more rapidly as a function of temperature than that of iron. It is quite unlikely that this rapid variation could be accounted for by the motion of the spins, as it would seem that the neighbouring spins in nickel are correlated as in the case of iron. This fact actually leads to the tenth power law of magnetic anisotropy of nickel with the additional dependence coming about because of the coupling constants themselves are the function of temperature. The tenth power law of the magnetic anisotropy agrees reasonably well with the experiment if the first anisotropy constant K_1 has a linear dependence on temperature. According to Breunner, some linear dependence of K_1

upon temperature should exist due to thermal expansion. The change in sign of K_1 at $\frac{T}{T_C} = 0.6$ is a key point toward understanding the anisotropy of Nickel.

Appendix

Table 3: Data for the measurement of torque at room temperature (298K)

Applied magnetic field H=1 kilo gauss	
Angle θ in degree	Torque τ in volt
0	-0.67
10	3.82
20	6.18
30	5.92
40	3.80
50	0.12
60	-2.44
70	-4.19
80	-3.90
90	-0.99
100	4.04
110	6.11
120	5.93
130	3.95
140	0.71
150	-1.95
160	-3.70
170	-3.45
180	-0.58
190	4.03
200	6.70
210	6.40
220	4.00
230	0.85
240	-2.00
250	-4.01
260	-3.90
270	-0.76
280	4.10
290	6.60
300	6.26
310	4.17
320	1.20
330	-1.58
340	-4.15
350	-3.87
360	-0.26

Table 4: Data for the measurement of torque at room temperature (298K)

Applied magnetic field $H=2$ kilo gauss	
Angle θ in degree	Torque τ in volt
0	-1.55
10	3.14
20	5.81
30	5.69
40	3.22
50	-0.70
60	-4.10
70	-5.95
80	-5.15
90	-1.62
100	3.28
110	6.05
120	5.90
130	3.70
140	0.11
150	-3.17
160	-5.00
170	-4.65
180	-1.52
190	2.70
200	5.38
210	5.27
220	2.79
230	-0.73
240	-4.01
250	-5.77
260	-5.12
270	-1.78
280	3.25
290	5.50
300	5.38
310	2.99
320	-0.11
330	-3.28
340	-5.17
350	-4.54
360	-1.20

Table 5: Data for the measurement of torque at room temperature (298K)

Applied magnetic field H=3 kilo gauss	
Angle θ in degree	Torque τ in volt
0	-1.45
10	3.20
20	5.85
30	5.80
40	3.30
50	-0.89
60	-4.30
70	-5.81
80	-5.20
90	-1.71
100	3.00
110	5.73
120	5.85
130	3.50
140	-0.56
150	-3.80
160	-5.57
170	-4.83
180	-1.50
190	3.20
200	5.90
210	5.75
220	3.30
230	-0.85
240	-4.25
250	-5.99
260	-5.07
270	-1.68
280	3.05
290	5.84
300	5.75
310	3.40
320	-0.59
330	-3.86
340	-5.46
350	-4.76
360	-1.40

Table 6: Data for the measurement of torque at room temperature (298K)

Applied magnetic field H=4 kilo gauss	
Angle θ in degree	Torque τ in volt
0	-1.35
10	3.10
20	5.41
30	5.40
40	2.90
50	-0.95
60	-4.47
70	-5.74
80	-5.18
90	-1.77
100	2.94
110	5.80
120	5.47
130	3.40
140	-0.52
150	-3.86
160	-5.60
170	-4.76
180	-1.44
190	3.10
200	5.55
210	5.35
220	2.87
230	-0.75
240	-4.31
250	-5.99
260	-4.98
270	-1.62
280	2.96
290	5.55
300	5.35
310	2.30
320	-0.66
330	-4.10
340	-5.26
350	-4.75
360	-1.40

Table 7: Data for the measurement of torque at 326K

Applied magnetic field H=1 kilo gauss	
Angle θ in degree	Torque τ in volt
0	-0.82
10	2.20
20	3.80
30	3.59
40	2.01
50	-0.53
60	-2.55
70	-3.65
80	-3.25
90	-1.04
100	2.20
110	3.88
120	3.80
130	2.50
140	-0.15
150	-2.05
160	-3.25
170	-3.00
180	-0.92
190	2.25
200	3.85
210	3.62
220	2.05
230	-0.46
240	-2.50
250	-3.65
260	-3.25
270	-0.97
280	2.25
290	3.95
300	3.80
310	2.35
320	-0.16
330	-2.15
340	-3.35
350	-2.95
360	-0.86

Table 8: Data for the measurement of torque at 326K

Applied magnetic field H=2 kilo gauss	
Angle θ in degree	Torque τ in volt
0	-0.78
10	2.30
20	4.05
30	4.00
40	2.10
50	-0.55
60	-2.80
70	-3.92
80	-3.32
90	-1.07
100	2.10
110	4.15
120	4.20
130	2.50
140	-0.02
150	-2.12
160	-3.42
170	-3.01
180	-0.84
190	1.95
200	4.10
210	3.95
220	2.01
230	-0.36
240	-2.85
250	-3.78
260	-3.22
270	-0.95
280	1.85
290	4.12
300	4.10
310	2.80
320	-0.09
330	-2.09
340	-3.35
350	-2.84
360	-0.55

Table 9: Data for the measurement of torque at 326K

Applied magnetic field $H=3$ kilo gauss	
Angle θ in degree	Torque τ in volt
0	-1.09
10	2.03
20	3.87
30	3.85
40	2.09
50	-0.99
60	-3.40
70	-4.52
80	-3.80
90	-1.54
100	1.95
110	3.90
120	3.95
130	2.35
140	-0.49
150	-2.85
160	-3.98
170	-3.49
180	-1.11
190	2.90
200	3.95
210	3.80
220	1.95
230	-0.85
240	-3.25
250	-4.35
260	-3.67
270	-1.34
280	1.85
290	3.80
300	3.75
310	2.10
320	-0.62
330	-2.80
340	-3.93
350	-3.30
360	-1.11

Table 10. Data for the measurement of torque at 326K

Applied magnetic field H=4 kilo gauss	
Angle θ in degree	Torque τ in volt
0	-0.56
10	2.39
20	4.10
30	4.12
40	2.52
50	-0.40
60	-2.70
70	-3.82
80	-3.10
90	-0.92
100	2.19
110	3.94
120	4.02
130	2.55
140	-0.17
150	-2.30
160	-3.34
170	-2.83
180	-0.70
190	2.26
200	3.93
210	3.97
220	2.45
230	-0.35
240	-2.63
250	-3.67
260	-3.00
270	-0.89
280	2.12
290	3.85
300	3.93
310	2.50
320	-0.15
330	-2.24
340	-3.28
350	-2.66
360	-0.60

Table II. Data for the measurement of torque at 351K

Applied magnetic field H=1 kilo gauss	
Angle θ in degree	Torque τ in volt
0	-0.43
10	1.96
20	3.17
30	3.04
40	1.86
50	-0.27
60	-1.84
70	-2.62
80	-2.32
90	-0.72
100	1.93
110	3.24
120	3.22
130	2.19
140	0.17
150	-1.34
160	-2.30
170	-2.12
180	-0.52
190	1.95
200	3.18
210	3.05
220	1.87
230	-0.20
240	-1.77
250	-2.65
260	-2.35
270	-0.57
280	1.96
290	3.34
300	3.21
310	2.12
320	0.09
330	-1.44
340	-2.31
350	-2.08
360	-0.48

Table 12: Data for the measurement of torque at 351K

Applied magnetic field H=2 kilo gauss	
Angle θ in degree	Torque τ in volt
0	-0.42
10	1.96
20	3.25
30	3.26
40	2.04
50	-0.26
60	-2.04
70	-2.86
80	-2.40
90	-0.74
100	1.85
110	3.26
120	3.34
130	2.29
140	0.11
150	-1.49
160	-2.43
170	-2.13
180	-0.49
190	1.98
200	3.27
210	3.28
220	2.05
230	-0.21
240	-1.96
250	-2.85
260	-2.40
270	-0.65
280	1.90
290	3.30
300	3.35
310	2.24
320	0.08
330	-1.56
340	-2.47
350	-2.08
360	-0.46

Table 13: Data for the measurement of torque at 351K

Applied magnetic field H=3 kilo gauss	
Angle θ in degree	Torque τ in volt
0	-0.40
10	1.85
20	3.20
30	3.30
40	1.90
50	-0.34
60	-2.05
70	-2.85
80	-2.30
90	-0.65
100	1.90
110	3.35
120	3.30
130	1.90
140	0.16
150	-1.40
160	-2.30
170	-2.01
180	-0.02
190	2.10
200	2.98
210	3.01
220	1.77
230	-0.10
240	-1.90
250	-2.80
260	-2.20
270	-0.50
280	1.80
290	2.97
300	3.04
310	1.95
320	0.22
330	-1.50
340	-2.40
350	-2.10
360	-0.08

Table 14: Data for the measurement of torque at 351K

Applied magnetic field H=4 kilo gauss	
Angle θ in degree	Torque τ in volt
0	-0.35
10	1.80
20	3.05
30	3.10
40	1.90
50	-0.20
60	-2.10
70	-2.75
80	-2.17
90	-0.50
100	1.72
110	3.13
120	3.30
130	2.19
140	0.25
150	-1.35
160	-2.28
170	-2.16
180	-0.25
190	2.00
200	3.05
210	3.01
220	1.65
230	-0.15
240	-1.95
250	-2.85
260	-2.45
270	-0.60
280	1.75
290	3.01
300	3.00
310	1.85
320	0.44
330	-1.45
340	-2.60
350	-2.55
360	-0.10

Table 15: Data for the measurement of torque at 374K

Applied magnetic field H=1 kilo gauss	
Angle θ in degree	Torque τ in volt
0	-0.45
10	1.38
20	2.34
30	2.27
40	1.35
50	-0.35
60	-1.58
70	-2.20
80	-1.90
90	-0.60
100	1.44
110	2.46
120	2.50
130	1.68
140	0.14
150	-1.00
160	-1.74
170	-1.57
180	-0.39
190	1.55
200	2.50
210	2.42
220	1.50
230	-0.21
240	-1.41
250	-2.06
260	-1.80
270	-0.52
280	1.58
290	2.59
300	2.38
310	1.76
320	0.17
330	-1.05
340	-1.80
350	-1.57
360	-0.40

Table 16: Data for the measurement of torque at 374K

Applied magnetic field H=2 kilo gauss	
Angle θ in degree	Torque τ in volt
0	-0.26
10	1.54
20	2.44
30	2.46
40	1.61
50	-0.13
60	-1.45
70	-2.02
80	-1.70
90	-0.43
100	1.47
110	2.46
120	2.55
130	1.83
140	0.25
150	-0.90
160	-1.60
170	-1.50
180	-0.22
190	1.59
200	2.48
210	2.49
220	1.63
230	-0.08
240	-1.34
250	-1.96
260	-1.63
270	-0.42
280	1.24
290	2.56
300	2.63
310	1.59
320	0.23
330	-0.99
340	-1.64
350	-1.37
360	-0.22

Table 17: Data for the measurement of torque at 374K

Applied magnetic field H=3 kilo gauss	
Angle θ in degree	Torque τ in volt
0	-0.15
10	1.20
20	2.20
30	2.25
40	1.30
50	-0.31
60	-1.55
70	-2.13
80	-1.77
90	-0.62
100	0.91
110	2.10
120	2.30
130	1.32
140	-0.01
150	-1.10
160	-1.70
170	-1.50
180	-0.40
190	1.10
200	2.35
210	2.30
220	1.30
230	-0.30
240	-1.40
250	-1.99
260	-1.63
270	-0.55
280	1.05
290	2.25
300	2.35
310	1.50
320	0.01
330	-1.01
340	-1.50
350	-1.45
360	-0.10

Table 18: Data for the measurement of torque at 374K

Applied magnetic field $H=4$ kilo gauss	
Angle θ in degree	Torque τ in volt
0	-0.04
10	1.55
20	2.60
30	2.65
40	1.65
50	-0.04
60	-1.30
70	-1.85
80	-1.50
90	-0.40
100	1.10
110	2.30
120	2.50
130	1.80
140	0.16
150	-0.80
160	-1.40
170	-1.20
180	-0.15
190	1.50
200	2.50
210	2.60
220	1.60
230	-0.60
240	-1.25
250	-1.85
260	-1.50
270	-0.40
280	1.25
290	2.45
300	2.60
310	1.80
320	0.20
330	-0.95
340	-1.52
350	-1.20
360	-0.14

Table 19: Data for the measurement of torque at 404K

Applied magnetic field $H=1$ kilo gauss	
Angle θ in degree	Torque τ in volt
0	-0.18
10	0.95
20	1.72
30	1.68
40	0.83
50	-0.16
60	-0.95
70	-1.50
80	-1.30
90	-0.35
100	0.81
110	1.85
120	1.90
130	1.40
140	0.25
150	-0.60
160	-1.08
170	-1.00
180	-0.22
190	0.97
200	1.75
210	1.70
220	0.83
230	-0.15
240	-0.97
250	-1.50
260	-1.35
270	-0.40
280	0.88
290	1.80
300	1.85
310	1.35
320	0.22
330	-0.65
340	-1.18
350	-1.02
360	-0.24

Table 20: Data for the measurement of torque at 404K

Applied magnetic field H=2 kilo gauss	
Angle θ in degree	Torque τ in volt
0	-0.07
10	0.76
20	1.45
30	1.43
40	0.79
50	-0.10
60	-0.97
70	-1.38
80	-1.16
90	-0.38
100	0.62
110	1.34
120	1.42
130	1.00
140	0.24
150	-0.45
160	-0.82
170	-0.85
180	-0.11
190	0.80
200	1.42
210	1.45
220	0.85
230	-0.05
240	-0.87
250	-1.30
260	-1.05
270	-0.28
280	0.78
290	1.45
300	1.50
310	1.05
320	0.28
330	-0.50
340	-0.98
350	-0.83
360	-0.12

Table 21: Data for the measurement of torque at 404K

Applied magnetic field H=3 kilo gauss	
Angle θ in degree	Torque τ in volt
0	-0.04
10	0.78
20	1.33
30	1.35
40	0.85
50	-0.07
60	-0.85
70	-1.25
80	-1.01
90	-0.25
100	0.70
110	1.55
120	1.70
130	1.20
140	0.30
150	-0.27
160	-0.67
170	-0.75
180	-0.10
190	0.75
200	1.35
210	1.40
220	0.82
230	-0.06
240	-0.75
250	-1.28
260	-0.89
270	-0.18
280	0.78
290	1.42
300	1.51
310	1.10
320	0.19
330	-0.40
340	-0.80
350	-0.65
360	0.05

Table 22. Data for the measurement of torque at 404K

Applied magnetic field H=4 kilo gauss	
Angle θ in degree	Torque τ in volt
0	0.16
10	0.95
20	1.50
30	1.51
40	0.93
50	0.03
60	-0.80
70	-1.20
80	-0.95
90	-0.25
100	0.68
110	1.52
120	1.60
130	1.12
140	0.30
150	-0.28
160	-0.60
170	-0.53
180	0.12
190	0.96
200	1.51
210	1.52
220	0.99
230	0.12
240	-0.70
250	-1.06
260	-0.87
270	-0.13
280	0.75
290	1.39
300	1.49
310	1.08
320	0.36
330	-0.33
340	-0.68
350	-0.52
360	0.14

Table 23. Data for the measurement of torque at 433K

Applied magnetic field H=1 kilo gauss.	
Angle θ in degree	Torque τ in volt
0	-0.20
10	0.45
20	1.25
30	1.20
40	0.40
50	-0.25
60	-0.80
70	-1.15
80	-1.10
90	-0.35
100	0.40
110	1.15
120	1.20
130	0.70
140	0.10
150	-0.58
160	-0.86
170	-0.91
180	-0.33
190	0.42
200	0.90
210	0.86
220	0.45
230	-0.25
240	-0.85
250	-1.18
260	-1.05
270	-0.40
280	0.42
290	0.98
300	1.05
310	0.70
320	0.08
330	-0.48
340	-0.88
350	-0.79
360	-0.28

Table 24: Data for the measurement of torque at 433K

Applied magnetic field $H=2$ kilo gauss	
Angle θ in degree	Torque τ in volt
0	-0.11
10	0.46
20	0.85
30	0.88
40	0.49
50	-0.14
60	-0.70
70	-0.96
80	-0.81
90	-0.30
100	0.37
110	0.78
120	0.90
130	0.66
140	0.18
150	-0.33
160	-0.68
170	-0.73
180	-0.26
190	0.32
200	0.73
210	0.76
220	0.36
230	-0.10
240	-0.69
250	-0.94
260	-0.81
270	-0.28
280	0.41
290	0.73
300	0.80
310	0.67
320	0.18
330	-0.35
340	-0.67
350	-0.58
360	-0.11

Table 25: Data for the measurement of torque at 433K

Applied magnetic field $H=3$ kilo gauss	
Angle θ in degree	Torque τ in volt
0	-0.06
10	0.44
20	0.68
30	0.70
40	0.34
50	-0.09
60	-0.61
70	-0.85
80	-0.70
90	-0.26
100	0.34
110	0.76
120	0.86
130	0.62
140	0.16
150	-0.35
160	-0.60
170	-0.50
180	-0.18
190	0.40
200	0.78
210	0.80
220	0.43
230	-0.14
240	-0.64
250	-0.88
260	-0.87
270	-0.30
280	0.32
290	0.63
300	0.71
310	0.46
320	0.00
330	-0.34
340	-0.64
350	-0.56
360	-0.10

Table 26: Data for the measurement of torque at 433K

Applied magnetic field H=4 kilo gauss	
Angle θ in degree	Torque τ in volt
0	-0.08
10	0.40
20	0.75
30	0.77
40	0.43
50	-0.07
60	-0.54
70	-0.77
80	-0.65
90	-0.25
100	0.27
110	0.68
120	0.78
130	0.54
140	0.16
150	-0.32
160	-0.60
170	-0.55
180	-0.06
190	0.45
200	0.76
210	0.78
220	0.42
230	-0.21
240	-0.70
250	-0.92
260	-0.81
270	-0.36
280	0.19
290	0.58
300	0.64
310	0.40
320	-0.01
330	-0.42
340	-0.65
350	-0.54
360	-0.11

Table 27: Data for the measurement of torque at 446K

Applied magnetic field H=1 kilo gauss	
Angle θ in degree	Torque τ in volt
0	
10	-0.13
20	0.45
30	0.86
40	0.81
50	0.39
60	-0.19
70	-0.71
80	-0.978
90	-0.87
100	-0.33
110	0.40
120	0.88
130	0.97
140	0.67
150	0.15
160	-0.18
170	-0.52
180	-0.47
190	-0.17
200	0.48
210	0.88
220	0.83
230	0.42
240	-0.16
250	-0.70
260	-0.95
270	-0.86
280	-0.31
290	0.43
300	0.91
310	0.98
320	0.66
330	-0.38
340	-0.72
350	-0.64
360	-0.16

Table 28: Data for the measurement of torque at 446K

Applied magnetic field H=2 kilo gauss	
Angle θ in degree	Torque τ in volt
0	0.07
10	0.55
20	0.88
30	0.89
40	0.55
50	-0.01
60	-0.60
70	-0.81
80	-0.68
90	-0.24
100	0.32
110	0.71
120	0.79
130	0.60
140	0.19
150	-0.05
160	-0.33
170	-0.28
180	0.08
190	0.57
200	0.89
210	0.90
220	0.55
230	0.04
240	-0.44
250	-0.66
260	-0.54
270	-0.09
280	0.49
290	0.87
300	0.94
310	0.74
320	0.32
330	-0.10
340	-0.37
350	-0.32
360	0.06

Table 29: Data for the measurement of torque at 446K

Applied magnetic field H=3 kilo gauss	
Angle θ in degree	Torque τ in volt
0	0.13
10	0.54
20	0.81
30	0.82
40	0.52
50	0.05
60	-0.50
70	-0.71
80	-0.60
90	-0.24
100	0.25
110	0.59
120	0.66
130	0.49
140	0.15
150	-0.02
160	-0.23
170	-0.18
180	0.13
190	0.55
200	0.83
210	0.84
220	0.53
230	0.08
240	-0.35
250	-0.55
260	-0.44
270	-0.05
280	0.44
290	0.78
300	0.85
310	0.67
320	0.33
330	-0.04
340	-0.25
350	-0.18
360	0.14

Table 30: Data for the measurement of torque at 446K

Applied magnetic field $H=4$ kilo gauss	
Angle θ in degree	Torque τ in volt
0	0.18
10	0.55
20	0.79
30	0.79
40	0.51
50	0.08
60	-0.37
70	-0.63
80	-0.55
90	-0.23
100	0.18
110	0.50
120	0.58
130	0.42
140	0.32
150	0.03
160	-0.15
170	-0.10
180	0.19
190	0.56
200	0.79
210	0.78
220	0.51
230	0.07
240	-0.31
250	-0.48
260	-0.37
270	-0.03
280	0.40
290	0.72
300	0.79
310	0.63
320	0.30
330	-0.02
340	-0.20
350	-0.12
360	0.17

Table 31: Data for the measurement of torque at 454K

Applied magnetic field H=1 kilo gauss	
Angle θ in degree	Torque τ in volt
0	-0.03
10	0.47
20	0.78
30	0.72
40	0.31
50	-0.21
60	-0.66
70	-0.87
80	-0.77
90	-0.27
100	0.42
110	0.86
120	0.93
130	0.67
140	0.19
150	-0.31
160	-0.55
170	-0.52
180	-0.11
190	0.47
200	0.83
210	0.77
220	0.36
230	-0.17
240	-0.65
250	-0.87
260	-0.77
270	-0.29
280	0.38
290	0.86
300	0.92
310	0.64
320	0.18
330	-0.30
340	-0.61
350	-0.55
360	-0.11

Table 32: Data for the measurement of torque at 454K

Applied magnetic field H=2 kilo gauss	
Angle θ in degree	Torque τ in volt
0	0.01
10	0.40
20	0.69
30	0.67
40	0.35
50	-0.12
60	-0.56
70	-0.75
80	-0.64
90	-0.25
100	0.29
110	0.65
120	0.74
130	0.58
140	0.22
150	-0.14
160	-0.38
170	-0.36
180	-0.03
190	0.40
200	0.71
210	0.72
220	0.39
230	-0.08
240	-0.53
250	-0.73
260	-0.63
270	-0.23
280	0.30
290	0.68
300	0.76
310	0.57
320	0.20
330	-0.19
340	-0.44
350	-0.39
360	-0.04

Table 33: Data for the measurement of torque at 454K

Applied magnetic field H=3 kilo gauss	
Angle θ in degree	Torque τ in volt
0	0.04
10	0.41
20	0.66
30	0.66
40	0.37
50	-0.06
60	-0.48
70	-0.67
80	-0.58
90	-0.26
100	0.19
110	0.51
120	0.59
130	0.45
140	0.22
150	-0.07
160	-0.27
170	-0.26
180	0.02
190	0.40
200	0.66
210	0.65
220	0.36
230	-0.06
240	-0.46
250	-0.64
260	-0.54
270	-0.19
280	0.27
290	0.59
300	0.66
310	0.51
320	0.19
330	-0.14
340	-0.34
350	-0.28
360	0.02

Table 34: Data for the measurement of torque at 454K

Applied magnetic field H=4 kilo gauss	
Angle θ in degree	Torque τ in volt
0	0.08
10	0.42
20	0.65
30	0.64
40	0.36
50	-0.05
60	-0.43
70	-0.61
80	-0.52
90	-0.20
100	0.20
110	0.49
120	0.57
130	0.43
140	0.19
150	-0.06
160	-0.21
170	-0.18
180	0.08
190	0.44
200	0.66
210	0.65
220	0.37
230	-0.03
240	-0.40
250	-0.58
260	-0.49
270	-0.18
280	0.25
290	0.55
300	0.62
310	0.47
320	0.18
330	-0.12
340	-0.29
350	-0.21
360	0.07

Table 35: Data for the measurement of torque at 463K

Applied magnetic field H=1 kilo gauss	
Angle θ in degree	Torque τ in volt
0	-0.25
10	0.28
20	0.55
30	0.45
40	0.05
50	-0.40
60	-0.80
70	-0.95
80	-0.98
90	-0.70
100	-0.05
110	0.45
120	0.65
130	0.40
140	-0.04
150	-0.45
160	-0.71
170	-0.72
180	-0.41
190	0.15
200	0.60
210	0.50
220	0.09
230	-0.39
240	-0.70
250	-0.90
260	-0.96
270	-0.70
280	-0.07
290	0.50
300	0.70
310	0.42
320	0.00
330	-0.41
340	-0.70
350	-0.71
360	-0.40

Table 36: Data for the measurement of torque at 463K

Applied magnetic field H=2 kilo gauss	
Angle θ in degree	Torque τ in volt
0	-0.21
10	0.16
20	0.44
30	0.41
40	0.10
50	-0.32
60	-0.63
70	-0.83
80	-0.85
90	-0.60
100	-0.15
110	0.34
120	0.50
130	0.39
140	0.06
150	-0.27
160	-0.50
170	-0.57
180	-0.35
190	0.08
200	0.43
210	0.45
220	0.14
230	-0.27
240	-0.61
250	-0.82
260	-0.84
270	-0.67
280	-0.23
290	0.27
300	0.45
310	0.36
320	0.05
330	-0.27
340	-0.52
350	-0.59
360	-0.40

Table 37: Data for the measurement of torque at 463K

Applied magnetic field H=3 kilo gauss	
Angle θ in degree	Torque τ in volt
0	-0.30
10	0.05
20	0.33
30	0.37
40	0.12
50	-0.20
60	-0.41
70	-0.62
80	-0.70
90	-0.62
100	-0.40
110	0.07
120	0.34
130	0.35
140	0.13
150	-0.17
160	-0.37
170	-0.50
180	-0.41
190	-0.09
200	0.25
210	0.39
220	0.19
230	-0.10
240	-0.37
250	-0.60
260	-0.75
270	-0.73
280	-0.56
290	-0.17
300	0.27
310	0.35
320	-0.09
330	-0.32
340	-0.46
350	-0.45
360	-0.25

Table 38: Data for the measurement of torque at 463K

Applied magnetic field H=4 kilo gauss	
Angle θ in degree	Torque τ in volt
0	-0.14
10	0.17
20	0.31
30	0.16
40	-0.09
50	-0.22
60	-0.44
70	-0.56
80	-0.60
90	-0.64
100	-0.68
110	-0.72
120	-0.74
130	-0.68
140	-0.42
150	0.20
160	0.09
170	-0.22
180	-0.35
190	-0.40
200	-0.34
210	-0.12
220	0.27
230	0.31
240	0.05
250	-0.20
260	-0.30
270	-0.51
280	-0.65
290	-0.75
300	-0.77
310	-0.67
320	-0.41
330	0.00
340	0.20
350	0.09
360	-0.14

Table 39: Data for the measurement of torque at 478K

Applied magnetic field H=1 kilo gauss	
Angle θ in degree	Torque τ in volt
0	0.72
10	0.43
20	0.05
30	-0.27
40	-0.42
50	-0.22
60	0.23
70	0.65
80	0.78
90	0.60
100	0.19
110	-0.21
120	-0.51
130	-0.61
140	-0.38
150	0.12
160	0.60
170	0.78
180	0.74
190	0.46
200	0.12
210	-0.23
220	-0.35
230	-0.18
240	0.26
250	0.67
260	0.78
270	0.66
280	0.25
290	-0.20
300	-0.50
310	-0.57
320	-0.34
330	0.16
340	0.64
350	0.84
360	0.77

Table 40: Data for the measurement of torque at 478K

Applied magnetic field $H=2$ kilo gauss	
Angle θ in degree	Torque τ in volt
0	0.65
10	0.52
20	0.24
30	0.02
40	-0.10
50	0.01
60	0.30
70	0.55
80	0.69
90	0.56
100	0.24
110	-0.11
120	-0.34
130	-0.38
140	-0.24
150	0.10
160	0.44
170	0.64
180	0.68
190	0.51
200	0.26
210	0.00
220	-0.09
230	0.02
240	0.32
250	0.58
260	0.68
270	0.59
280	0.24
290	-0.13
300	-0.35
310	-0.37
320	-0.22
330	0.11
340	0.47
350	0.64
360	0.68

Table 41: Data for the measurement of torque at 478K

Applied magnetic field H=3 kilo gauss	
Angle θ in degree	Torque τ in volt
0	0.59
10	0.48
20	0.30
30	0.11
40	0.04
50	0.15
60	0.39
70	0.58
80	0.65
90	0.53
100	0.27
110	-0.03
120	-0.25
130	-0.27
140	-0.15
150	0.09
160	0.37
170	0.55
180	0.59
190	0.50
200	0.32
210	0.13
220	0.06
230	0.14
240	0.36
250	0.55
260	0.64
270	0.55
280	0.28
290	-0.02
300	-0.23
310	-0.27
320	-0.14
330	0.11
340	0.38
350	0.58
360	0.62

Table 42: Data for the measurement of torque at 478K

Applied magnetic field H=4 kilo gauss	
Angle θ in degree	Torque τ in volt
0	0.57
10	0.51
20	0.34
30	0.18
40	0.11
50	0.20
60	0.38
70	0.56
80	0.62
90	0.51
100	0.30
110	-0.01
120	-0.21
130	-0.26
140	-0.13
150	0.09
160	0.32
170	0.52
180	0.56
190	0.48
200	0.31
210	0.15
220	0.09
230	0.18
240	0.35
250	0.55
260	0.60
270	0.49
280	0.27
290	-0.01
300	-0.21
310	-0.22
320	-0.10
330	0.11
340	0.37
350	0.54
360	0.58

Table 43: Data for the measurement of torque at 498K

Applied magnetic field H=1 kilo gauss	
Angle θ in degree	Torque τ in volt
0	0.77
10	0.55
20	0.25
30	-0.04
40	-0.16
50	-0.01
60	0.37
70	0.67
80	0.78
90	0.64
100	0.25
110	-0.08
120	-0.33
130	-0.40
140	-0.22
150	0.20
160	0.61
170	0.78
180	0.76
190	0.54
200	0.25
210	-0.02
220	-0.15
230	-0.02
240	0.31
250	0.66
260	0.78
270	0.63
280	0.27
290	-0.09
300	-0.33
310	-0.40
320	-0.20
330	0.20
340	0.60
350	0.77
360	0.75

Table 44: Data for the measurement of torque at 498K

Applied magnetic field H=2 kilo gauss	
Angle θ in degree	Torque τ in volt
0	0.63
10	0.54
20	0.34
30	0.14
40	0.05
50	0.14
60	0.34
70	0.56
80	0.65
90	0.54
100	0.28
110	-0.01
120	-0.21
130	-0.24
140	-0.09
150	0.15
160	0.42
170	0.58
180	0.62
190	0.54
200	0.34
210	0.14
220	0.07
230	0.16
240	0.38
250	0.56
260	0.64
270	0.54
280	0.26
290	-0.02
300	-0.22
310	-0.22
320	-0.09
330	0.16
340	0.52
350	0.62
360	0.63

Table 45 Data for the measurement of torque at 498

Applied magnetic field H=3 kilo gauss	
Angle θ in degree	Torque τ in volt
0	0.56
10	0.51
20	0.38
30	0.23
40	0.17
50	0.22
60	0.37
70	0.51
80	0.55
90	0.50
100	0.28
110	0.03
120	-0.13
130	-0.16
140	-0.07
150	0.11
160	0.33
170	0.47
180	0.53
190	0.49
200	0.38
210	0.26
220	0.18
230	0.23
240	0.38
250	0.51
260	0.55
270	0.46
280	0.25
290	0.02
300	-0.15
310	-0.17
320	-0.06
330	0.16
340	0.38
350	0.52
360	0.57

Table 46 Data for the measurement of torque at 498K

Applied magnetic field H=4 kilo gauss	
Angle θ in degree	Torque τ in volt
0	0.52
10	0.50
20	0.40
30	0.28
40	0.23
50	0.28
60	0.38
70	0.48
80	0.50
90	0.42
100	0.27
110	0.06
120	-0.07
130	-0.11
140	-0.04
150	0.11
160	0.30
170	0.44
180	0.49
190	0.46
200	0.37
210	0.27
220	0.22
230	0.28
240	0.41
250	0.50
260	0.52
270	0.42
280	0.23
290	0.02
300	-0.09
310	-0.11
320	0.03
330	0.12
340	0.32
350	0.45
360	0.51

References

- [1] N. Akulov, *Z. Physik* 100, 197 (1936).
- [2] C. Zener, *Phys. Rev.* 96, 1335 (1954).
- [3] Robert Brenner, *Phys. Rev* 107, 1539 (1957).
- [4] J. H. Van Vleck, *Phys. Rev.* 52, 1178 (1937).
- [5] F. Keffer, *Phys. Rev.* 100, 1692 (1955).
- [6] L. Pal, *Acta. Phys Acad. Hung. Sci.* 3, 287 (1954).
- [7] J. H. Van Vleck, *J. Phys. radium* 20, 124 (1959).
- [8] F. Keffer and T. Oguchi, *Phys. Rev.* 117, 718 (1960).
- [9] Frederic Keffer, *Phys. Rev.* 100, 1692 (1955).
- [10] R. R. Birss and P. M. Wallis, *J. of Applied Physics* 39, 1347 (1968).
- [11] H. B. Callen and E. Callen, *J. Phys. Chem. Solids.* 27, 1271-1285 (1966).
- [12] J. J. M. Franse and G. De Vries, *Physica* 39, 477-498 (1968).
- [13] R. R. Birss, G. J. Keeler and P. D. Leo, *JMMM* 15-18, 571-572.(1980).
- [14] R. M. Bozorth, *Phys. Rev.* 50, 1076-1081 (1936).
- [15] L. P. Tarasov, *Phys. Rev.* 56, 1224-1230 (1939).
- [16] R. M. Bozorth and H. J. Williams, *Phys. Rev.* 59, 827 (1941).
- [17] C. D. Graham, Jr, *Phys. Rev.* 112, 1117 (1958).
- [18] W. J. Carr, Jr, *J of Applied Physics* 31, 69 (1960).
- [19] C. Kittel and J. H. Van Vleck, *Phys. Rev.* 118, 1231 (1960)
- [20] R. Becker and W. Döring, *Ferromagnetismus* (Verlag-Julius pringer, Berlin, 1939) P. 136.
- [21] W. J. Carr, Jr., *Phys. Rev.* 108, 1158 (1957).
- [22] F. C. Powell, *Proc. Roy. Soc (London)* A130, 167 (1930).
- [23] F. Bloch and G. Gentile, *Z. Physik* 70, 395 (1931).
- [24] Van Vleck, *Physica* 5, 465 (1938).
- [25] H. Brooks, *Phys. Rev.* 58, 909 (1940).
- [26] G. C. Fletcher, *Proc. Phys. Soc. (London)* A67, 505 (1954).

- [27] W. J. Carr, Jr., Phys. Rev. 109, 1971 (1958).
- [28] F. C. Nix and D. MacNair, Phys. Rev. 60, 597 (1941).
- [29] F. Simon and R. Bergmann, Zeits. f. physik. Chemie B8, 225 (1930).
- [30] [13] L. P. Tarasov, Phys. Riv. 56, 1239 (1939).
- [31] N. S. Akulov, Zeits. f. Physik 57, 249 (1929)
- [32] E. R. Jette and E. S. Greiner, Trans. A. I. M. E. 105, 259 (1933).
- [33] Hiroshi Sato and B. S. Chandrasekhar, J. Phys. Chem Solids. 1, 228-233 (1957)
- [34] C. Lottel, Phys. Rev. 118, 5 (1960).
- [35] L. Néel, R. Pauthenet, G. Rimet, and V. S. Giron, J. of Applied Physics 31. 27S (1960).
- [36] L. Néel, Ann. Phys., 18, 5 (1932); 5. 232 (1936).
- [37] F. Bitter, Phys. Rev. 54. 79 (1937).
- [38] J. H. van Vleck, J. Chem. Phys., 9, 85 (1941).
- [39] H. Bizette, C. F. Squire, and B. Tsai, Compt. rend., 207, 449 (1938).
- [40] B. Westerstrandh, U. Gafvert and L. Lundgren, Physics Scripta. 14, 5-10 (1976).
- [41] M. A. Mazid, M. Amanullah Chowdhury and Shireen Akter, Internal Report (1986)
- [42] G. W. Van Oesterhout, Appl. Sci. Rev. B6, 101 (1965).
- [43] S. Foner, Rev. Sci. Instr. 30, 548-557 (1959).
- [44] S. Foner, Rev. Sci. Instr. 27, 578 (1955).
- [45] F. A. Khan, M. A. Asgar, P. Nordblad, JMMM, 174, 121-126, 1997.
- [46] T. Jonsson, J. Mattsson, C. Djurberg, F. A. Khan, P. Nordblad and P. Svedlindh, Phys. Rev. Letters, 75, 4138, 1995.
- [47] F. A. Khan, Ph.D. Thesis, BUET, 1995
- [48] P. Nordblad. Ph.D. Thesis, Uppsala University 1981.

